

Title	The effect of hydrogeological and hydrochemical dynamics on landslide triggering in the central highlands of Ethiopia
Authors	Mebrahtu, T. K.;Banning, Andre;Girmay, E. H.;Wohnlich, S.
Publication date	2021-02-12
Original Citation	Mebrahtu, T.K., Banning, A., Girmay, E.H. and Wohnlich, S. (2021) 'The effect of hydrogeological and hydrochemical dynamics on landslide triggering in the central highlands of Ethiopia', Hydrogeology Journal, 29, pp. 1239–1260. doi: 10.1007/s10040-020-02288-7
Type of publication	Article (peer-reviewed)
Link to publisher's version	https://link.springer.com/article/10.1007%2Fs10040-020-02288-7 - 10.1007/s10040-020-02288-7
Rights	© The Authors 2021. Open Access. This article is licensed under a Creative Commons Attribution 4.0 International License. - http://creativecommons.org/licenses/by/4.0/
Download date	2024-04-25 15:04:56
Item downloaded from	https://hdl.handle.net/10468/12259



The effect of hydrogeological and hydrochemical dynamics on landslide triggering in the central highlands of Ethiopia

Tesfay Kiros Mebrahtu¹ · Andre Banning¹ · Ermias Hagos Girmay² · Stefan Wonnlich¹

Received: 26 February 2020 / Accepted: 6 December 2020 / Published online: 12 February 2021
© The Author(s) 2021

Abstract

The volcanic terrain at the western margin of the Main Ethiopian Rift in the Debre Sina area is known for its slope stability problems. This report describes research on the effects of the hydrogeological and hydrochemical dynamics on landslide triggering by using converging evidence from geological, geomorphological, geophysical, hydrogeochemical and isotopic investigations. The chemical characterization indicates that shallow to intermediate aquifers cause groundwater flow into the landslide mass, influencing long-term groundwater-level fluctuations underneath the landslide and, as a consequence, its stability. The low content of total dissolved solids and the bicarbonate types (Ca-Mg-HCO_3 and Ca-HCO_3) of the groundwater, and the dominantly depleted isotopic signature, indicate a fast groundwater flow regime that receives a high amount of precipitation. The main causes of the landslide are the steep slope topography and the pressure formed during precipitation, which leads to an increased weight of the loose and weathered materials. The geophysical data indicate that the area is covered by unconsolidated sediments and highly decomposed and weak volcanic rocks, which are susceptible to sliding when they get moist. The heterogeneity of the geological materials and the presence of impermeable layers embodied within the highly permeable volcanic rocks can result in the build-up of hydrostatic pressure at their interface, which can trigger landslides. Intense fracturing in the tilted basalt and ignimbrite beds can also accelerate infiltration of water, resulting to the build-up of high hydrostatic pressure causing low effective normal stress in the rock mass, giving rise to landslides.

Keywords Landslides · Stable isotopes · Triggering mechanisms · Hydrochemistry · Ethiopia

Introduction

Rainfall-triggered landslides occur frequently in the central highlands of Ethiopia. These highlands are highly populated regions in which more than 60% of the country's population is settled. The mean annual rainfall in these regions exceeds 1,200 mm and accounts for some 70% of the total precipitation the country receives each year (Ayalew 1999). The highlands are highly rugged. The topographical variation, land-use, geology, and the surface water and groundwater flow systems here are strongly characteristic for this type of region, as are rainfall-

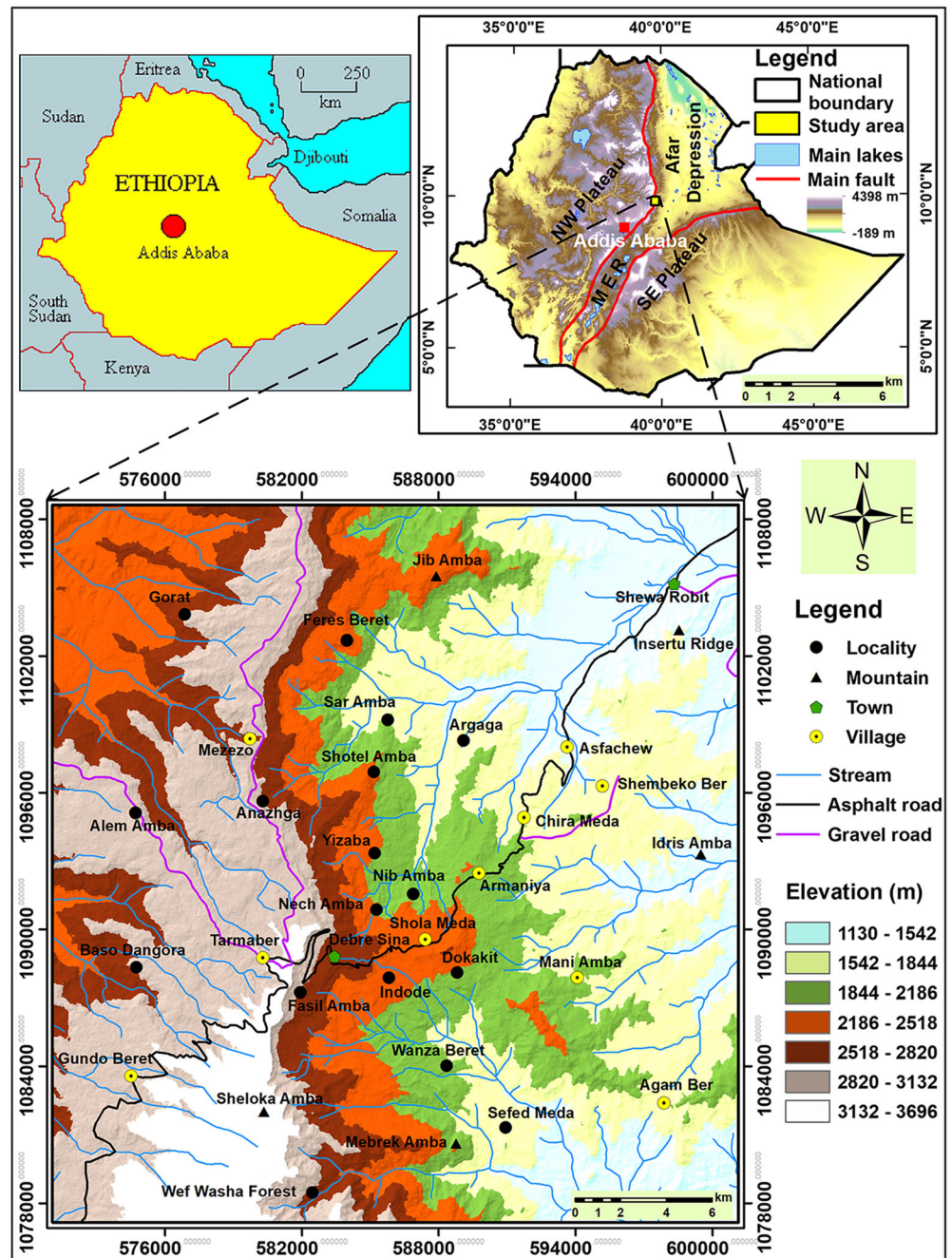
triggered landslides (Woldearegay 2013). Most of the landslides in these highland regions, including the largest ones, are triggered by heavy precipitation occurring at the end of the rainy periods in July and August (Ayalew 1999). In addition, fast-moving slope failures such as rock slides, occur due to seismic triggering by earthquakes from the Afar depression (Fig. 1), the Main Ethiopian Rift (MER) and their escarpments (Abebe et al. 2010). There were also reactivated landslides during the fieldwork in this research conducted from April to June 2016 and October to November 2017, following heavy rainfall and earthquake incidents. Rainfall-induced mass movement hazards in the Debre Sina area are closely linked with hydro-meteorological hazards such as slope instability and erosion. This is shown by the strong association of landslides with streams or river incision and with gully erosion. During the past few years, natural disasters within the central highlands of Ethiopia have increased in both frequency and intensity, and have had severe social impacts. According to previous studies (e.g., Ayalew 1999; Temesgen et al. 2001; Ayalew and Yamagishi 2002; Ayenew and Barbieri 2005; Woldearegay

✉ Tesfay Kiros Mebrahtu
tesfay.mebrahtu@rub.de

¹ Department of Applied Geology, Ruhr University Bochum, Institute of Geology, Mineralogy and Geophysics, D-44780 Bochum, Germany

² Mekelle University, School of Earth Sciences, P.O. Box 3006, Mekelle, Ethiopia

Fig. 1 Location map of the study area



et al. 2005), the landslides have severely affected human lives, infrastructures, agricultural lands, and the natural environment in various parts of the highlands and rift margins of Ethiopia. Besides rising public awareness of the landslide hazard, there has been little to no changes in land-use or other protective measures in this region.

Hydrogeological data, and hence hydrogeological assessment, on the large-scale and deep-seated landslides are extremely scarce in the study area and other parts of the central highlands of Ethiopia. The infiltration of precipitation into the subsurface is one of the main factors that initiates and controls

the mobilization of rock (Iverson 2000). Groundwater-level rise is often the critical factor for slope failure because it induces high pore-water pressures which can reduce the frictional strength of slopes. As stated by different researchers (e.g., Bogaard et al. 2000; Tullen et al. 2002; Malet 2003; Lindenmaier et al. 2005), large landslides usually imply a complex hydrogeology with various flow paths. Defining the origin, age and ongoing processes of groundwater flow while it passes through a landslide area, can contribute to understanding the hazard (de Montety et al. 2007). Hydrogeochemistry can also be an important contribution to

characterize landslides, as hydrogeochemistry and isotope ratios can be characteristic (Epstein and Mayeda 1953; Tóth 1999; Guglielmi et al. 2000; Wang et al. 2001; Guglielmi et al. 2002; de Montety et al. 2007; Cervi et al. 2012). Groundwater that flows within volcanic rocks alters the chemical composition of the groundwater itself, with influences from the precipitation, mineralogy of the watershed aquifers, climate, topography, and anthropogenic and volcanic activities (Edmunds et al. 1992). The interaction of groundwater with these factors leads to the formation of different hydrochemical facies which can be correlated with location, geology, climatic conditions and topography (Clark and Fritz 1997). A number of research projects in different countries have shown that the patterns of hydrogeochemistry and $\delta^{18}\text{O}$ and $\delta^2\text{H}$ isotopic compositions in the water can provide a useful tool for landslide investigations (Di Maio et al. 2004, 2014; Gaucher et al. 2006; Picarelli et al. 2006; de Montety et al. 2007; Calmels et al. 2011; Cervi et al. 2012; Vallet et al. 2015), while there have been no similar studies undertaken in Ethiopia and particularly in the Debre Sina area, where the study area resides.

Landslide incidences in the central highlands of Ethiopia and the western margin of the Ethiopian Rift escarpment are increasing at an alarming rate. Therefore, investigation of hydrogeological dynamics is vital for understanding the influence of water on the potential to move mass. Nevertheless, hydrogeological data associated with large-scale and deep-seated landslides are extremely scarce in the study area. Considering the scale of the landslide problems and the socio-economic development in the area, there is an urgent need to understand the hydrological processes, to evaluate the soil/rock–water interactions and to determine the nature of sliding movements. These are essential for appropriate hazard maps and realistic predictions, as well as for developing systems for early warning of landslide hazards in the margins of the western Afar depression. The study area is hardly accessible and the active movement of landslides may quickly destroy instrumentation. Therefore, to identify the most relevant influencing factors, a comprehensive study of the geology, groundwater flow conditions, respective rock–water interactions, and geophysical investigations was conducted. Thus, the objective of this study is to implement a converging evidence approach towards understanding the main landslide triggering factors and the land-mass failure mechanisms through (1) detailed study of the geological and structural settings of the study area by using remote sensing data, field geological mapping and geophysical techniques (2) conceptualization of the hydrological processes and rock–water interactions by using hydrogeochemical and isotope approaches and (3) integration of the geological, hydrogeological, hydrogeochemical and isotope data. The data presented and the issues raised in this report will also be useful for similar studies across the East African Rift and in similar tectonic settings.

The study area

The study area is located in the central-western highlands of Ethiopia, forming spectacular escarpments along the margins of the southwestern Afar depression, which is tectonically active (Fig. 1). It is geographically bounded by UTM 1077165 m N and 1,108,635 m N, and the UTM 571065 m E and 601,125 m E. The steep escarpment and the narrow strip of the plateau over-look the Afar depression. The steep mountain chains and rugged valleys that drain into the central-eastern and western lowlands of Ethiopia characterize the wider area. The elevation ranges from 1,130 m above sea level (asl) in the southeast and northeast parts, to 3,696 m near Tarmaber on the plateau (Fig. 1). The high-elevation ridge chain occupies the western part of the study area and represents the area's highest peaks. It includes highly elevated and N–S trending outstanding ridge chains with steep cliff escarpments.

The Ethiopian highland is characterized by variable climatic conditions. The climate of the study area is significantly colder and wetter than the rest of Ethiopia due to the high elevation and high gradient. The area has subhumid to humid climate and bi-modal type of rainfall (rainy months: March to mid-May and mid-June to September). The annual rainfall distribution is characterized by pronounced seasonality, with the heaviest rains occurring in July and August. The area has an annual average precipitation of about 1,812 mm which is estimated based on 43 years of complete precipitation records (Mebratu et al. 2020a). In general, the western highlands bounding the Rift Valley receives high rainfall, above 1,200 mm/year, whilst the rift floor gets little seasonal rain, often less than 600 mm/year. The air temperature has a maximum value of 25 °C and a minimum value of 10 °C, whereas the mean annual temperature is 15 °C. The lower and middle parts of the area are densely populated and massively cultivated. People in this region are still actively involved in agriculture. The area is characterized by deeply dissected valleys and channels, rugged relief, mesas, plains, high-elevation continuous ridge chains with steep cliff escarpments, highly variable topographic features and complex geology, which reflect the past geological and erosional processes (Mebratu et al. 2020b). This implies that the area is subjected to dynamic geomorphic processes of erosion, transportation, and material deposition. Stream networks originate in the highlands, and then they proceed further outwards through deep gorges towards the rift valley. The drainage pattern is well defined with parallel to subparallel dendritic patterns developed along faults and master joints in the hard rocks.

Intensive rainfall induces fast-moving slope failures, which have affected the Debre Sina area several times in recent years. The increasing impact of anthropogenic activities (land-use changes, especially deforestation and intensive agriculture, quarrying, road construction, urbanization, etc.) has

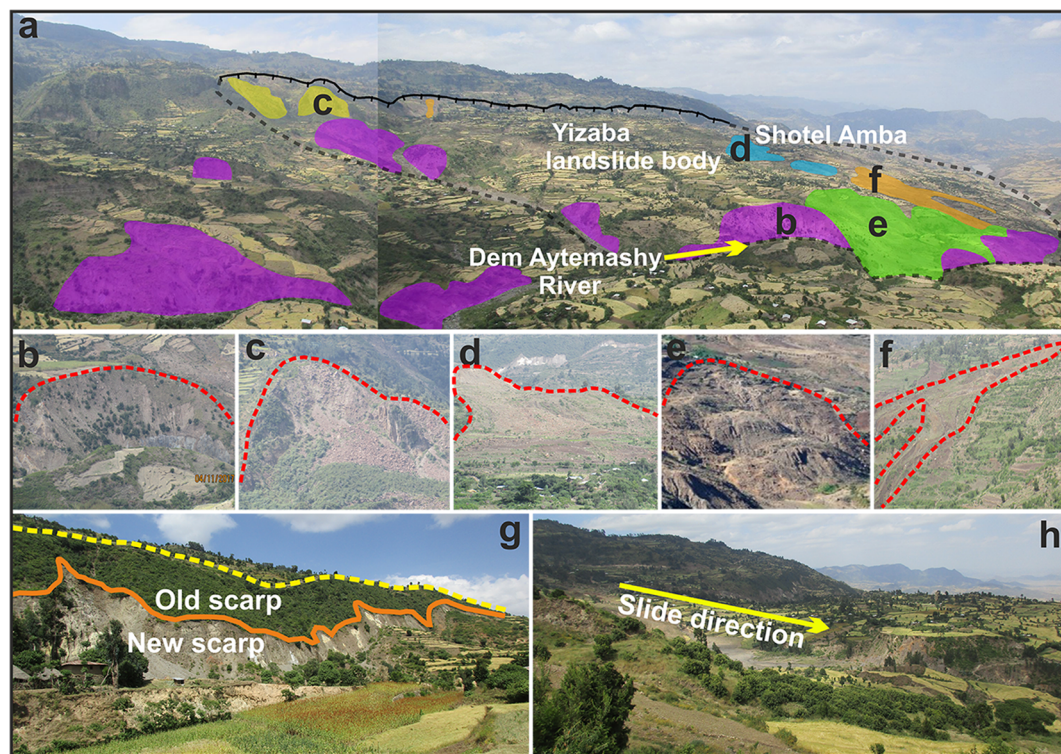


Fig. 2 **a** Panoramic view of the main Yizaba and Shotel Amba landslides from the east, with examples of characteristic geodynamic features within the main landslide body and its surroundings: **b** rotational slide, **c** rock

slide, **d** debris/earth slide, **e** debris flow, **f** earth flow, **g** translational slide occurred in 2005 and **h** large-scale sliding

also contributed to slope instability and landslide hazards over the last two decades (e.g., Ayalew 2000; Nyssen et al. 2003; Zvelebil et al. 2010). Settlements at the foot of steep slopes and close to the streams that carry flood flows and debris from adjacent mountains are especially in danger. As mentioned by Woldearegay (2008), the localities Yizaba Wein and Shotel Amba areas were strongly affected by a single major deep-seated landslide that took place on 13 September 2005 and the slope instability problem still remains very active (Fig. 2). The Debre Sina landslide that reactivated during summer 2005 had existed for the previous 15 years. Since the original landslide activity started, the slide has continued to move at a relatively high rate. The most common types of landslides in this area are rotational slides, translational slides, rockfalls and toppling, rock slides, debris slides, and debris and earth flows (Fig. 2).

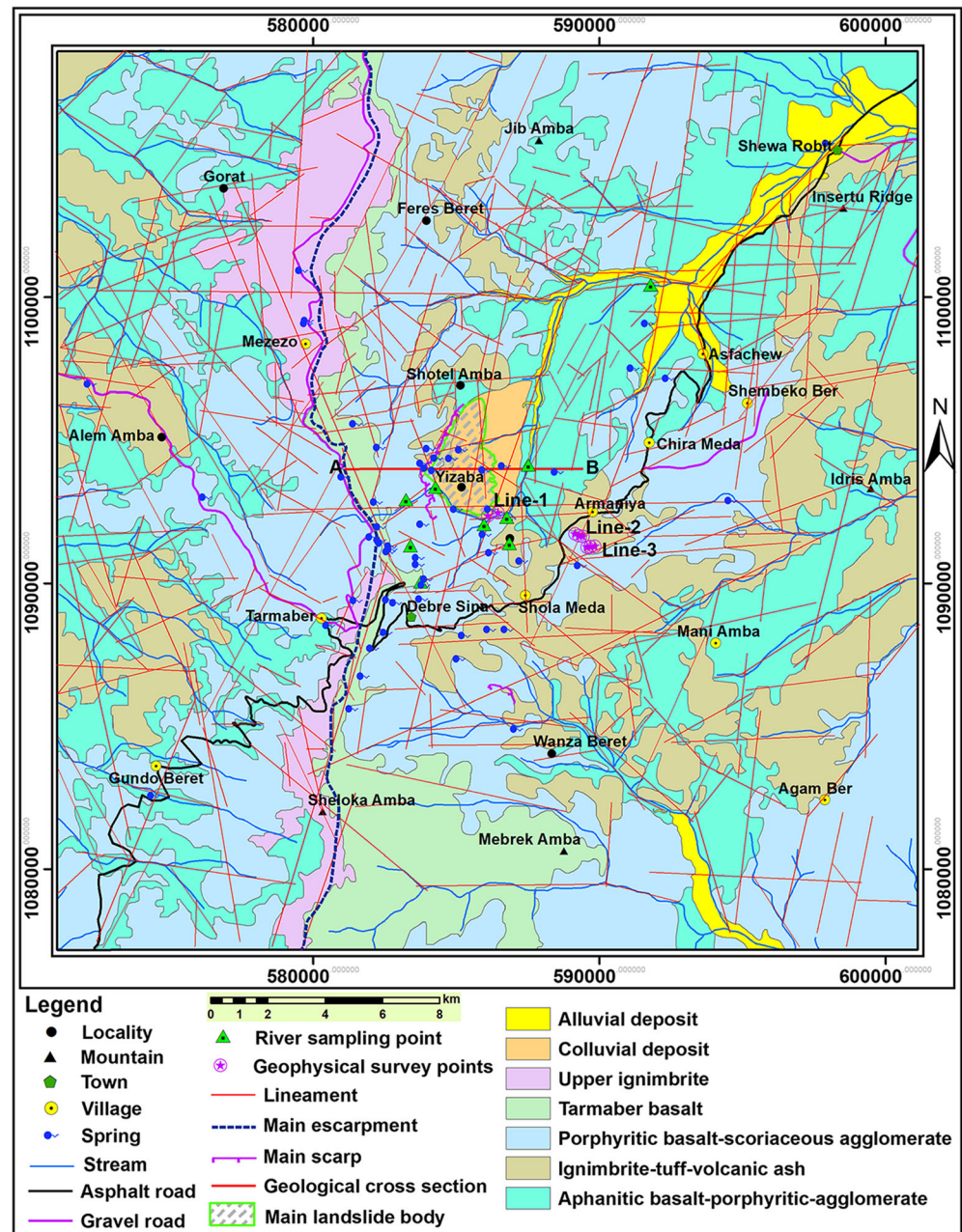
Geological setting

The study area is marked by its complex lithological and tectonic settings. The Cenozoic era is characterized by extensive faulting accompanied by widespread volcanic activity and uplift. The area is represented by two major litho-stratigraphic formations, which are the Tertiary volcanic rocks associated with volcanic ash and the Quaternary superficial deposits. The major rock and soil types in the area include: aphanitic basalt,

porphyritic basalt and agglomerate basalt (aphanitic basalt–porphyritic–agglomerate); ignimbrite–tuff–volcanic ash; intercalated porphyritic basalt and scoriaceous agglomerate (porphyritic basalt–scoriaceous agglomerate); Tarmaber basalt; upper ignimbrite; and unconsolidated deposits (colluvial and alluvial deposits; Fig. 3). The volcanic rocks have experienced intense weathering, which resulted in the occurrence of deep weathering profiles and weathered landforms. The aphanitic basalt–porphyritic–agglomerate units crop out in the gully areas and series of cliffs and benches in deeply dissected valleys. The unit exhibits notable textural and compositional variations vertically, which are constituted by the aphanitic basalt, porphyritic basalt, and scoriaceous agglomerate basalt.

The ignimbrite–tuff–volcanic ash unit mainly consists of pumiceous lapilli tuff and volcanic ash with subordinate ignimbrite, trachyte, and rhyolite. The ignimbrite–tuff–volcanic ash beds form small cliffs that are highly altered and intensely weathered, and are vertically jointed and highly shattered by faulting (Mebratu et al. 2020a). The porphyritic basalt–scoriaceous agglomerate unit consists of dominantly porphyritic basalt and scoriaceous agglomerate with subordinate aphanitic basalt and vesicular basalt. The porphyritic–scoriaceous agglomerate basalt shows a high rate of spheroidal weathering and breaks easily to very small-sized material, and the weathering and fracturing prevails more in the major

Fig. 3 Geological map of the study area (modified from Mebrahtu et al. 2020a)



joints and layering. This unit is highly weathered and fractured, favoring the circulation and storage of subsurface water. The Tarmaber basalt unit is mainly exposed in the western part of the study area in the high-rising mountain chains (Fig. 3). This rock formation forms vertical cliffs and ridges trending in the N–S direction as well as some E–W offsets and shows well-developed columnar joints (Mebrahtu et al. 2020a). The upper ignimbrite unit is exposed in the western part of the study area overlying the Tarmaber basalt. This unit is fine-grained, highly weathered, and crossed by subvertical to vertical fractures (Mebrahtu et al. 2020a).

The slopes with lower inclination are covered by Quaternary sediments. The colluvial deposits are associated

with rock pediments originating mainly from the basalt, presumably transported downslope by the action of gravity and slope wash (Mebrahtu et al. 2020a). These colluvial deposits mainly contain rock fragments and soil derived from fragmented and weathered bedrock. The alluvial sediments are deposited along the major riverbeds and convey large volumes of sediment during the wet season, mostly in the form of debris slides and flows. They are derived from the weathering, transportation, and reworking of different rocks from the steep cliffs and the escarpment. The area is traversed by four major trends of faults (N–S, E–W, NE–SW, and NW–SE; Fig. 3) and they can be assumed to be a major conduit for groundwater flow. However, this behavior can be sometimes lost or

sealed by precipitation of secondary material or clay (Guglielmi et al. 2000). The landslides coincide with the tectonically active geological structures.

Materials and methods

Water sampling and analytical methods

A multi-techniques investigation strategy combining hydro-geochemical, isotopic and geophysical methods, was followed in this study. Groundwater chemistry and stable isotopes analyses were used to characterize the groundwater flow system and rock–water interactions. The water samples were collected in two field campaigns (April–June 2016 and October–November 2017) from 65 sites. The samples were taken directly from two different sources, which include cold springs and rivers. Spring water samples were collected directly at their discharge points under natural pressure by using a plastic syringe. The water sampling point locations were systematically selected in order to be representative of: different rock formations in the stratigraphic column; recharge and discharge areas; and landslide areas and surroundings. The locations of the sample sites are shown in Fig. 3, and the hydrochemical results, including isotope data, are presented in Table 1. All the water samples were filtered through a 0.45- μm membrane on site and filled 50-ml polyethylene bottles. The samples taken for major cations analysis were acidified to pH 2 with HNO_3 (nitric acid). All the major ions except HCO_3^- were analysed using ion chromatography (Dionex 1000 Ion Chromatography System) in the laboratory of Applied Geology at the Ruhr University of Bochum (RUB), Germany. HCO_3^- was analysed in the field by employing a burette titration method by using HCl , and the total Fe (Fe_{tot}) was determined by atomic absorption spectrometry 240F (AAS) in the RUB. Measurements of electrical conductivity (EC), pH and temperature were made in-situ by using WTW Multi340i handheld meters, and each electrode was calibrated. Conventional field hydrogeological observations and a landslide inventory were done to support the results from hydrochemical and isotope analyses.

The stable isotopes (^{18}O and ^2H) were measured in 39 water samples (33 cold springs and 6 rivers). The sampling bottles were repeatedly rinsed with the water to be sampled and then completely filled leaving no space for air. Water samples for stable isotopes (^{18}O and ^2H) were collected in high-density polyethylene bottles (50 ml) and analyzed following standard procedures at the laboratory of Isodetec (Environmental Monitoring) in Munich and the Department of Materials and Earth Sciences at the Technical University of Darmstadt, Germany. The determination of ^{18}O and ^2H in groundwater was carried out by using a laser absorption device (PICARRO L2130-i $\delta\text{D}/\delta^{18}\text{O}$ Ultra High-Precision

analyzer). The measured values of the samples (mean of 10 individual measurements) were calibrated with international standards (Standard Light Antarctic Precipitation (SLAP), Standard Mean Ocean Water (SMOW), Greenland Ice Sheet Precipitation (GISP)) and any drift or memory effects were corrected. The general measurement error is ± 0.1 or $\pm 0.5\text{‰}$ (standard deviation) based on the Vienna Standard Mean Ocean Water (VSMOW). The measurement inaccuracy (simple standard deviation) of the analysis carried out reached a maximum of $\pm 0.09\text{‰}$ for ^{18}O and $\pm 0.3\text{‰}$ for ^2H . Long-term isotopic data of rainfall (from 1961 to 2016) from the Addis Ababa (Fig. 1) Global Network of Isotopes in Precipitation (GNIP) station (190 km from the study area) is taken from the International Atomic Energy Agency database (IAEA 2020). The resulting stable isotope data are interpreted by plotting them with the Global Meteoric Water Line (GMWL; Craig 1961), and the local meteoric water line (LMWL) of Addis Ababa (Kebede et al. 2008). In this study, Statistica version 8.0 was used to conduct hierarchical cluster analysis (HCA). The softwares *ArcGIS 10.5* (Esri), *Geochem* (US Geological Survey), computer program *Diagrammes v 6.5* and *CorelDRAW X7* were used for database creation, spatial data analysis and to prepare high-quality maps and illustrations. The final results and interpretations were then combined to formulate a conceptual hydrogeological model of the Debre Sina landslide area.

Geophysical survey

Data acquisition and processing

Vertical electrical soundings (VES) were applied to approximately delineate horizontally layered strata and to investigate the vertical layering. The electrical resistivity data were collected using the ABEM Terrameter SAS 4000/SAS 1000 with steel electrodes, cables on reels and other accessories. Four electrodes were placed along a straight line on the earth surface. Current was injected into the earth through two electrodes (A and B) and the resulting voltage differences were measured at two potential electrodes (M and N). The Schlumberger array (A M N B) was used, with the distance between current electrodes five times the one of the voltage electrodes. The VES was carried out on the profile lines with AB/2 and MN/2 spacing ranging from 1.5 to 220 m and 0.5 to 20 m, respectively. The resistivity data were collected at eight points, two of which were in the Yizaba area, while the remaining six were in the Armaniya area (Fig. 3). The apparent resistivity (ρ_a) data were then plotted against the electrode spacing (AB/2) in order to obtain a resistivity-depth model for iteration on the *IPI2win* software (IP2win 2003). The iterations were completed once an RMS error $< 5\%$ was obtained. The final RMS errors in this study vary between 1.59 and 4.41%. Finally, the results were interpreted both qualitatively

Table 1 Hydrochemical and isotope data of sampled groundwater and surface water in the Debre Sina area, SP spring, R river; Ionic concentrations are measured in mg/L

Sample ID	X	Y	Elev (m asl)	EC ($\mu\text{S}/\text{cm}$)	pH	T ($^{\circ}\text{C}$)	TDS (mg/L)	Li^+	Na^+	K^+	Mg^{++}	Ca^{++}	Fe_{tot}	HCO_3^-	F^-	Cl^-	NO_3^-	SO_4^-	$\delta^2\text{H}$ [‰]	$\delta^{18}\text{O}$ [‰]	d-excess [‰]
SP01	582,657	1,091,105	2850	131	7.5	18.0	181	0.1	5.5	1.1	5.4	13.5	0.1	145.0	0.1	1.0	7.9	1.3	-13.91	-5.08	26.80
SP02	582,895	1,089,302	2826	101	6.9	20.4	158	0.1	4.2	0.9	3.1	12.5	0.1	120.0	0.1	1.3	12.3	3.3	-8.27	-4.48	27.60
SP03	583,879	1,089,927	2616	115	7.4	17.1	131	0.5	7.8	3.0	3.0	12.0	0.2	90.0	0.2	1.6	8.8	3.9	-9.27	-4.36	25.60
SP04	583,689	1,090,650	2626	118	7.9	16.9	136	0.1	5.3	1.6	3.7	13.6	0.1	95.0	0.1	2.7	10.8	3.4	-5.49	-3.94	26.00
SP05	583,689	1,090,882	2585	113	7.6	16.9	168	0.1	5.0	1.5	3.7	13.4	0.1	130.0	0.1	1.9	9.7	3.0	-8.37	-4.15	24.80
SP06	585,290	1,088,159	2425	158	6.3	18.7	156	0.5	28.0	4.0	2.0	12.0	2.3	95.0	0.2	2.0	5.3	7.3	-5.91	-4.02	26.20
SP07	586,172	1,088,369	2316	259	6.6	20.9	234	0.1	9.1	3.4	9.1	30.1	0.1	150.0	0.1	5.0	19.4	7.5	-4.39	-3.72	25.40
SP08	586,780	1,088,368	2306	220	6.4	21.4	215	0.5	11.0	6.2	6.2	26.0	0.1	135.0	0.3	3.7	21.0	5.0	-5.53	-3.82	25.00
SP09	586,018	1,091,691	1975	307	8.1	24.2	399	0.1	15.8	6.9	9.8	34.4	0.1	310.0	0.3	3.4	12.0	6.6	-1.42	-2.91	21.80
SP10	586,202	1,092,581	2035	315	7.9	22.8	442	0.1	48.0	4.4	2.7	20.7	0.1	345.0	0.6	3.9	10.1	7.2	-3.86	-3.50	24.10
SP11	585,012	1,092,580	2129	153	8.0	20.0	220	0.5	8.3	3.0	5.0	19.0	0.1	160.0	0.4	2.6	17.0	4.1	-6.13	-4.02	26.10
SP12	585,193	1,094,664	2200	153	6.6	26.3	141	0.5	7.4	5.0	4.0	18.0	0.2	85.0	0.2	3.0	12.4	5.4	-5.78	-3.91	25.50
SP13	586,690	1,094,093	1887	215	6.5	23.1	195	0.5	14.0	4.0	5.9	25.0	0.1	120.0	0.6	4.8	13.5	7.4	-4.49	-3.06	20.00
SP14	588,535	1,093,884	1988	376	7.5	22.7	329	0.1	18.8	2.2	10.9	47.0	0.1	220.0	0.4	11.2	13.9	4.8	-	-	-
SP15	592,420	1,097,151	1531	544	7.2	25.3	423	0.5	26.0	4.0	14.0	64.4	0.1	260.0	0.3	12.6	28.0	13.1	2.39	-1.94	17.90
SP16	591,183	1,097,502	1473	418	8.4	25.8	343	0.5	35.0	5.3	12.0	48.0	0.1	210.0	0.6	8.8	8.7	14.7	8.21	-0.87	15.10
SP17	591,693	1,099,083	1549	542	8.3	28.4	427	0.1	52.5	1.0	18.0	40.0	0.1	235.0	1.0	17.0	41.0	22.0	7.64	-0.73	13.50
SP18	572,226	1,096,951	2934	155	7.3	17.8	123	0.5	7.0	0.5	4.0	17.0	0.1	83.0	0.3	3	7.5	1.0	-	-	-
SP19	589,347	1,090,612	2128	297	6.8	21.4	266	0.5	31.0	7.2	9.4	23.0	0.2	180.0	0.5	3.1	8.9	2.4	-3.74	-3.36	23.20
SP20	594,605	1,092,884	2125	286	7.2	25.8	419	0.5	21.0	5.0	8.4	40.0	0.1	310.0	0.4	10.1	10.6	13.5	-	-	-
SP21	582,566	1,088,267	2806	119	6.6	15.3	184	0.1	6.1	1.2	3.4	14.3	0.1	140.0	0.1	1.4	14.1	3.8	-	-	-
SP22	582,341	1,091,954	2826	139	7.6	15.7	216	0.1	5.9	1.9	4.1	17.6	0.1	155.0	0.1	1.4	28.0	1.6	-	-	-
SP23	582,218	1,092,826	2805	125	8.1	16.2	215	0.1	6.2	1.3	3.7	15.0	0.1	170.0	0.1	1.0	16.2	1.4	-9.96	-4.49	25.90
SP24	582,326	1,094,739	2580	99	8.1	17.8	172	0.1	5.0	1.9	3.3	11.3	0.1	140.0	0.1	1.6	6.5	2.4	-	-	-
SP25	581,491	1,095,576	2532	72	6.4	15.7	129	0.1	5.6	2.2	2.1	7.9	0.1	90.0	0.1	1.0	16.4	3.6	-	-	-
SP26	584,064	1,094,702	2420	185	7.7	16.3	108	0.5	5.8	2.8	4.0	15.0	0.1	73.2	0.2	3.3	0.1	3.0	-	-	-
SP27	584,335	1,094,375	2269	465	7.0	19.4	128	0.5	14	4.9	3	14	0.1	79	0.6	4.7	4.6	3.3	-3.9	-2.24	14.0
SP28	583,844	1,094,191	2416	183	6.6	18.7	137	0.5	6.7	2.9	4	16	0.1	70	0.2	2.9	31	2.6	-	-	-
SP29	583,980	1,094,020	2375	216	6.8	21.5	127	0.5	6.4	9.8	4	15	0.17	70	0.2	7.4	9	4.4	-5.9	-2.80	16.5
SP30	584,250	1,093,933	2317	207	6.5	21.3	121	0.5	5.9	7.7	4.0	17.0	0.5	61.0	0.2	3.8	4.4	16.9	-7.05	-2.96	16.64
SP31	584,847	1,094,360	2234	177	6.4	19.6	103	0.5	7.3	4.5	4.0	15.0	0.1	61.0	0.3	3.0	2.5	4.9	-5.92	-2.85	16.87
SP32	586,002	1,093,953	2073	373	7.0	22.0	262	0.5	16.0	1.1	9.5	38.0	0.1	189.1	0.3	2.2	0.1	5.7	-	-	-
SP33	583,842	1,092,047	2562	199	7.7	17.1	97	0.5	5.8	1.6	4.0	18.0	0.1	61.0	0.1	1.1	3.6	1.2	-	-	-
SP34	587,303	1,090,769	2167	205	8.0	16.8	109	0.5	6.0	2.4	5.0	17.0	0.1	73.2	0.2	1.5	0.1	3.3	-	-	-

Table 1 (continued)

Sample	X	Y	Elev (m asl)	EC ($\mu\text{S}/\text{cm}$)	pH	T ($^{\circ}\text{C}$)	TDS (mg/L)	Li^{+}	Na^{+}	K^{+}	Mg^{++}	Ca^{++}	Fe_{tot}	HCO_3^{-}	F^{-}	Cl^{-}	NO_3^{-}	SO_4^{-}	$\delta^2\text{H}$ [‰]	$\delta^{18}\text{O}$ [‰]	d- excess [‰]
ID																					
SP35	586,248	1,091,063	2143	307	9.8	21.3	201	0.5	11.0	3.1	8.1	30.0	0.1	140.3	0.3	1.9	0.7	4.0	-1.58	-2.18	15.84
SP36	587,111	1,084,884	1870	284	8.4	21.4	177	0.5	11.0	2.9	7.1	28.0	0.7	103.7	0.1	1.9	2.6	18.9	-3.11	-2.53	17.14
SP37	582,718	1,091,290	2864	177	7.6	14.8	99	0.5	5.0	1.4	4.0	16.0	0.1	67.1	0.1	1.4	2.4	1.4	-13.29	-4.10	19.53
SP38	583,970	1,090,132	2621	193	7.9	16.1	127	0.5	9.5	11.3	3.0	12.0	0.1	73.2	0.1	13.9	0.1	3.5	-11.03	-3.80	19.39
SP39	583,808	1,089,437	2642	222	7.9	17.5	141	0.5	11.0	2.0	5.1	19.0	0.1	97.6	0.1	2.3	2.2	1.2	-	-	-
SP40	581,361	1,085,598	2715	176	6.9	13.8	118	0.5	4.0	5.6	5.0	15.0	0.1	73.2	0.1	10.6	1.5	2.9	-10.10	-3.79	20.22
SP41	581,761	1,086,736	2821	155	6.9	13.4	97	0.5	4.0	0.6	3.0	13.0	0.1	67.1	0.1	2.7	3.9	1.8	-8.78	-3.54	19.54
SP42	582,096	1,087,709	2845	234	6.6	14.8	159	0.5	5.9	3.9	6.7	23.0	0.1	103.7	0.1	10.6	1.7	3.3	-8.73	-3.58	19.88
SP43	585,110	1,087,341	2424	294	6.9	22.4	191	0.5	8.6	2.0	8.4	30.0	0.1	115.9	0.2	9.1	12.3	4.2	-4.30	-2.53	15.95
SP44	580,555	1,088,521	3173	109	6.9	18.0	96	0.5	4.0	0.6	3.0	13.0	0.1	67.1	0.1	2.7	3.9	1.8	-15.20	-4.20	18.40
SP45	582,739	1,091,179	2960	173	7.4	17.0	115	0.5	5.2	1.0	3.8	15.0	0.1	85.4	0.1	0.9	2.7	0.9	-14.60	-4.10	18.20
SP46	598,008	1,105,381	1273	535	7.3	24.0	522	0.5	47.0	3.9	14.8	53.1	0.8	329.4	0.1	22.6	8.0	42.7	-1.20	-1.60	11.60
SP47	581,091	1,093,710	3113	94	6.6	16.3	63	0.5	3.0	0.5	2.0	10.0	0.1	16.0	0.1	7.0	20.0	4.0	-	-	-
SP48	579,777	1,099,074	2900	87	7.1	15.8	70	0.5	5.0	0.9	2.0	9.0	0.1	45.0	0.1	1.0	4.4	3.0	-	-	-
SP49	579,605	1,100,941	3005	83	6.9	18.0	61	0.5	2.0	2.0	1.0	8.0	0.1	35.0	0.1	3.0	4.4	6.0	-	-	-
SP50	579,807	1,099,181	2918	214	7.5	15.6	178	0.5	11.0	5.0	4.0	24.0	0.1	128.0	0.4	3.0	1.3	2.0	-	-	-
SP51	582,334	1,091,496	3021	141	7.4	17.2	113	0.5	5.0	0.6	4.0	17.0	0.1	79.0	0.2	1.0	5.8	1.0	-	-	-
SP52	576,252	1,093,000	3003	161	7.3	18.0	127	0.5	8.0	3.0	4.0	18.0	0.1	85.0	0.4	4.0	3.1	2.0	-	-	-
SP53	582,409	1,091,394	2979	172	8.0	17.0	138	0.5	6.0	2.0	5.0	19.0	0.1	98.0	0.3	4.0	0.4	4.0	-	-	-
SP54	581,506	1,089,390	3147	116	7.9	15.0	92	0.5	5.0	0.9	3.0	13.0	0.1	61.0	0.1	1.0	5.8	2.0	-	-	-
SP55	582,066	1,091,594	3058	160	8.0	18.0	127	0.5	7.0	2.0	4.0	19.0	0.1	89.0	0.3	3.0	2.2	1.0	-	-	-
SP56	582,643	1,089,410	2873	174	7.4	21.0	135	0.5	6.0	3.0	4.0	19.0	0.1	89.0	0.2	5.0	5.3	4.0	-	-	-
R01	583,771	1,090,042	2596	93	7.4	17.8	110	0.1	5.0	1.7	2.5	10.1	0.2	75.0	0.1	1.7	9.9	4.1	-4.21	-3.82	26.30
R02	583,413	1,091,305	2557	122	7.8	15.8	199	0.1	6.4	1.7	4.0	15.0	0.1	160.0	0.1	2.4	8.0	1.3	-11.46	-4.72	26.30
R03	586,865	1,091,394	2015	268	7.8	22.0	235	0.1	18.2	7.3	6.7	27.5	0.1	150.0	0.4	3.4	9.2	12.8	-1.69	-2.66	19.60
R04	586,773	1,092,303	1825	234	8.0	20.7	206	0.5	22.0	4.0	5.7	24.0	0.2	130.0	0.4	2.4	8.1	8.8	-2.84	-3.36	24.10
R05	587,526	1,094,130	1692	244	7.2	24.5	246	0.5	22.0	3.0	5.5	27.0	0.1	170.0	0.4	2.6	6.6	8.6	-	-	-
R06	583,253	1,092,922	2507	166	8.1	15.0	86	0.5	5.7	2.1	4.0	13.0	0.1	54.9	0.1	1.2	2.9	1.6	-	-	-
R07	584,282	1,093,360	2275	190	7.4	19.1	93	0.5	5.0	1.7	4.0	13.0	0.1	61.0	0.2	2.2	3.5	2.4	-5.34	-2.97	18.38
R08	585,977	1,092,051	1939	241	8.4	22.0	214	0.5	19.0	3.4	5.2	23.0	0.1	146.4	0.3	5.6	2.9	8.2	-4.01	-2.50	15.97
R09	591,792	1,100,433	1433	573	8.5	25.5	470	0.5	40.0	4.3	15.0	59.6	0.1	311.1	0.6	12.9	15.8	11.2	-	-	-

and quantitatively. In the quantitative interpretation, a pseudo-depth section and geo-electric section were created. The measured potential difference demonstrates the effects of different geological materials within the area. The raw resistivity data are plotted as a pseudo-depth section using the IPI2win software, which demonstrates the vertical variation of measured resistivity as a function of electrode spacing ($AB/2$) and guides the construction of the geo-electrical section using *surf-er 17* software and MATLAB. Based on the geo-electric sections, the subsurface structures are quantitatively characterized.

Results and discussion

Aquifer system and groundwater flow

The groundwater flow in the study area is controlled by geological structures, topography and rock type. The groundwater flow direction in the whole basin coincides with the topography following the surface-water flow direction (Fig. 4) because small intermittent and particularly perennial rivers form local drainage basins and shallow aquifers. The flow is partly controlled by the structure and partly by the geomorphology of the area; local groundwater flow directions vary from place to place according to the local topography (Fig. 4). The groundwater divide between the Rift Valley and the Jemma basin do not generally conform to the surface-water divide; the divide is slightly shifted to the west into the Jemma basin particularly in the northwestern part of the study.

The lithostratigraphic, geomorphologic, isotopic and hydrochemical evidence indicates that two groundwater flow systems (shallow/local and intermediate-deep) exist in the study area. The shallow groundwater flow is mainly localized to the highland areas and adjacent escarpments and its water table is a subdued replica of the surface topography (Figs. 5 and 6), which is generally characterized by lower concentrations of dissolved ions, depletion in heavy isotopes and higher d -excess. A significant part of the groundwater is discharged to rivers (in the form of baseflow) and as contact springs within the highland plateau and its margins. The intermediate-deep groundwater flow is strongly influenced by the lithostratigraphy and the major faults in the area rather than the surface geomorphology. At the top of the slope, groundwater directly flows through the vertical to subvertical joints with different flow paths mainly guided by the highly permeable gravitational features that correspond to interconnected tension cracks. This intermediate deep groundwater is recharged through the deep-seated fractures adjacent to the major faults in the highland plateaus and discharges mainly in the form of high-discharge springs and baseflow in the eastern lowland sections of the Dem Aytemashy, Robi, Majete and Shenkorge rivers (Figs. 4 and 6). The shallow

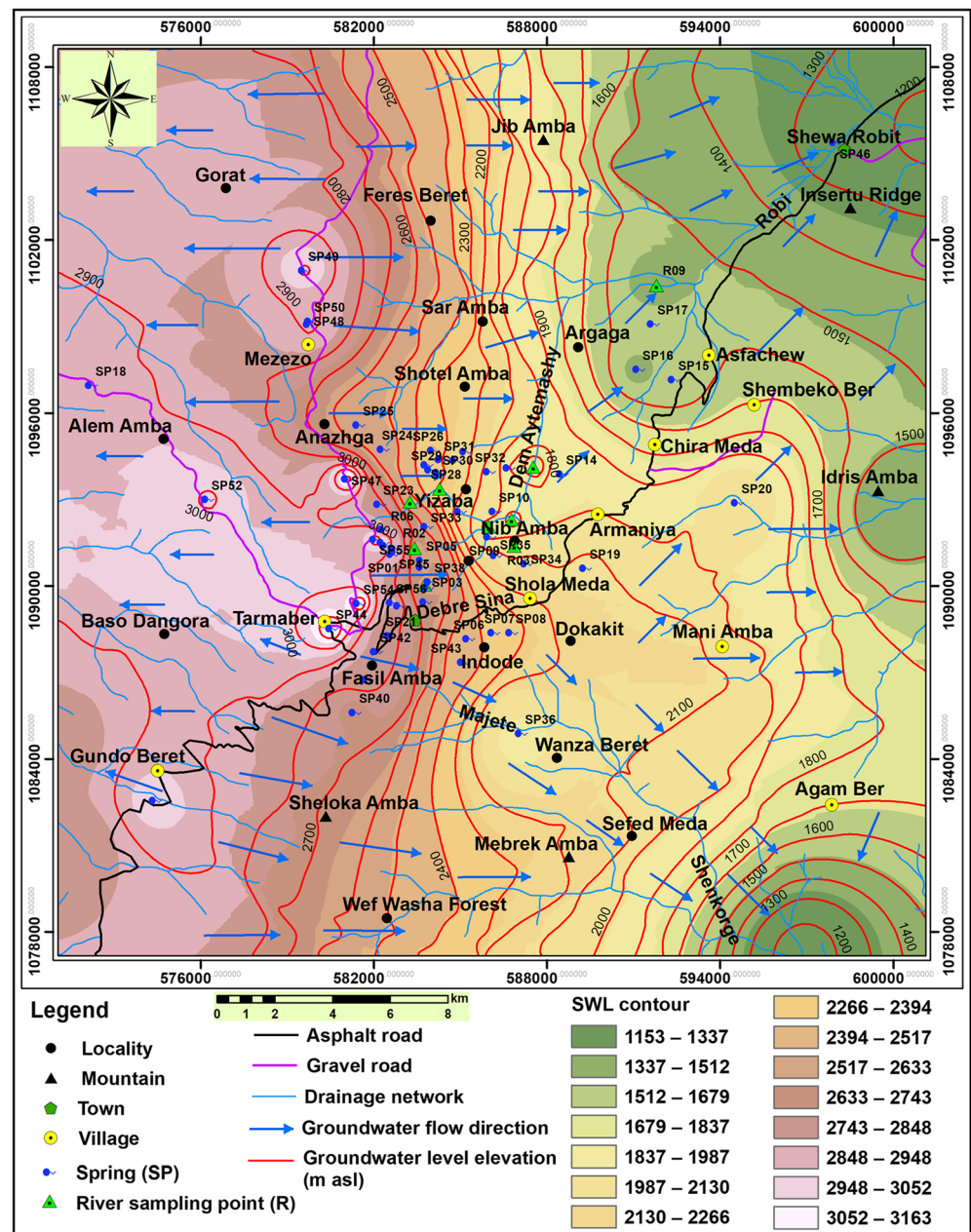
aquifer system is drained by the perennial springs located at the top of slopes, at the basal aquifer in the lower part of the slopes and at the landslide toe.

The Fig. 4 depicts that there is a swamp area (discharge of groundwater) around Argaga/Asfachew in the north-central part of the area, which corresponds well with field observations in the study area. This marshy area is developed where the rocks are impermeable and rock–water intact near the surface. Around Yizaba and Majete areas, the groundwater contours are closed indicating flow from all directions towards the center (Fig. 4). As the water table drops below the stream level, water infiltrates from streams and rivers into the aquifer. Aquifers along the rivers are recharged by the surface water of streams, and the flow of many streams is controlled by geological structure. The area is characterized by large faults that play important roles in the occurrence and movement of the groundwater. The plateau volcanic rocks retain rainwater for a long time and create favorable conditions for infiltration through a highly weathered, jointed and permeable upper layer. The shallow groundwater is partly drained by rivers and the remaining water recharges the underlying aquifers. The highly permeable fracture network facilitates subsurface flow to the lowlands as the primary recharge source of the deeper aquifers.

The highly fractured volcanic rock of the plateau, consisting of basalt, ignimbrite, rhyolite and/or trachyte, is one of the major water-bearing formations in the area. It also covers large gently-to-steeply undulating areas of the eastern part of the area. In accordance with to the distribution of springs (Fig. 3), the inter-bedded volcanic rocks of the ignimbrite–tuff–volcanic ash act as a semiconfined aquifer. The vertical to subvertical joints and tensional features in the Tarmaber basalt covering the plateau area create a favourable condition for rainwater percolation. Most springs are located at topographic breaks such as hillsides.

Generally, there is a clear zonation in the total ionic concentration of natural waters following the direction of groundwater flow from the highlands to the lower elevations. This zonation corresponds with the spatial variations of recharge and discharge conditions and the geological setting. The slight increase in the total ionic concentration towards the lowland implies that the residence time of the groundwater and the magnitude of rock–water interaction are likely to increase in the same direction. The faults in the area are not only weak zones, but also mostly characterized by deeper weathering and higher potential for concentrated groundwater flow, which can act as a lubricant and produce water pressure, causing landslides. The most favorable condition for landslides in the Debre Sina area and its surroundings is considered to be the fractured state of the bedrocks, especially near the tectonic lines. As a result, most mass movement occurs in the NNE–SSW and N–S directions, which coincides with set of lineaments. The lapilli tuff, tuff breccia and tuffaceous strata within the pyroclastic unit make the strata susceptible to slaking,

Fig. 4 Groundwater level map and groundwater flow directions based on spring and river positions. SWL static water level



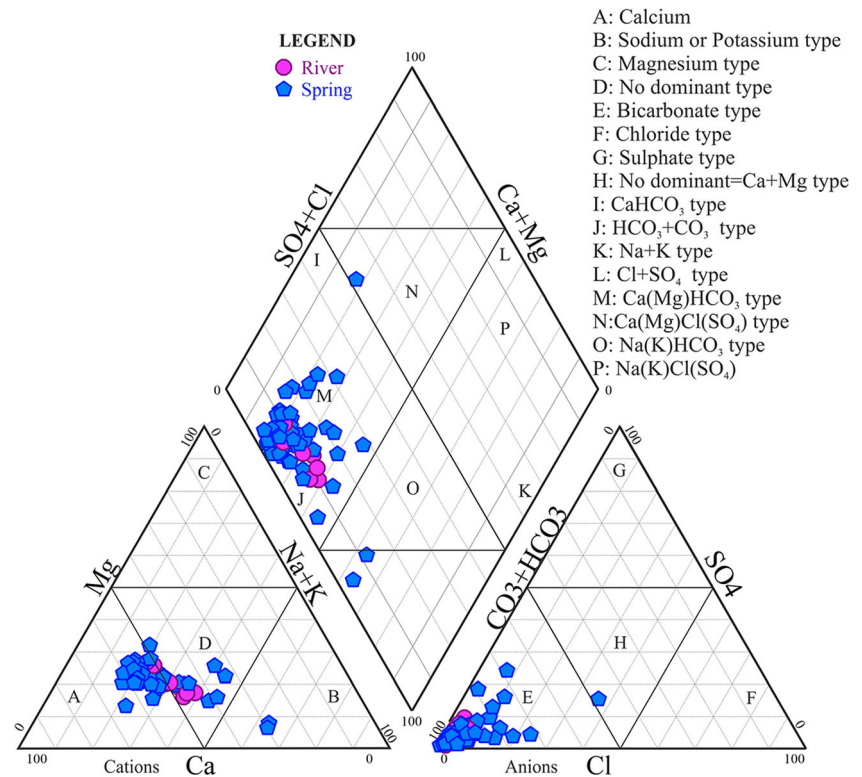
which, in itself, can also be one of the triggering factors of landslides in the area. Triggering mechanisms can also be aggravated by the development of pore-water pressure, seepage forces, seepage erosion and mechanisms related to high plasticity. The hydrogeological conditions of the terrains are generally favourable for the development of seepage forces within the pyroclastic sediments (tuff and pumice horizons) and unconsolidated deposits during periods of rainfall.

Hydrogeochemical facies

All the groundwaters and the surface waters in the area are fresh, characterized by low total dissolved solids (TDS)

ranging from 61 to 522 mg/L. The pH values show that the groundwater is slightly acidic to alkaline (6.3–9.8) in springs and rivers (Table 1). The chemical groundwater types of an area can be distinguished and grouped by their position in a Piper diagram (Piper 1944). Different hydrochemical facies were identified in the study area on the basis of the Piper diagram (Fig. 5), and four major water types, identified as Ca-Mg-HCO_3 , Ca-HCO_3 , Ca-Mg-Cl-SO_4 and Na-HCO_3 , classified according to their dominant chemical composition (Fig. 5) were found. Groundwater and surface water from the higher elevations typically have a $\text{Ca}^{2+}(\text{Mg}^{2+})\text{-HCO}_3^-$ hydrochemical facies, whereas groundwater in the lower altitude displays a $\text{Na}^+\text{-HCO}_3^-$ type (SP46). There is a general

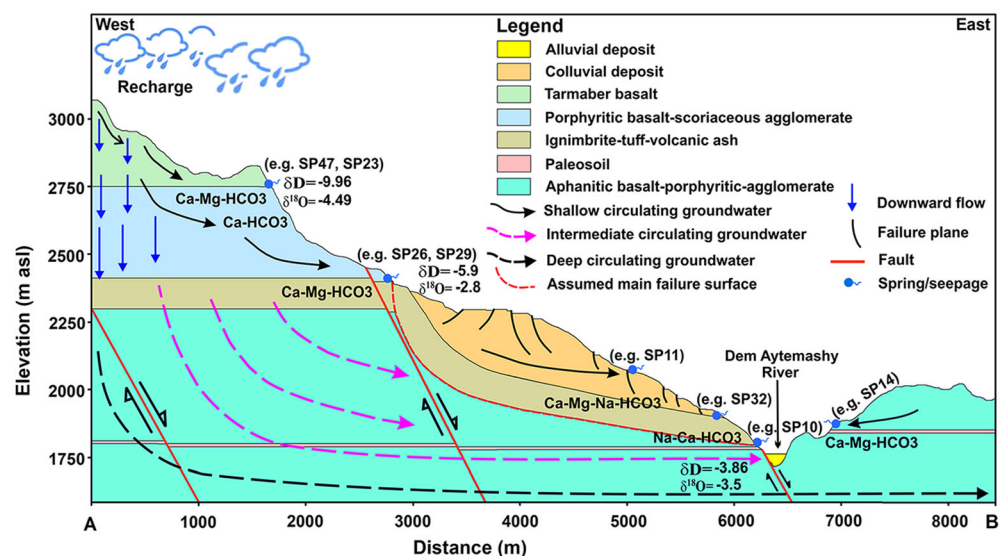
Fig. 5 Piper diagram showing compositions of different water types in the study area



compositional change from a $\text{Ca}^{2+}(\text{Mg}^{2+})\text{HCO}_3^-$ type water to a $\text{Na}^+\text{HCO}_3^-$ hydrochemical facies along the groundwater flow path from higher to lower altitude (Fig. 6). This result is consistent with other hydrochemical studies conducted along the central-western highlands and margins of the Afar depression (Darling et al. 1996; Chernet et al. 2001; Ayenew 2005). As topography controls the fluxes in the hydrological cycle, it also controls the hydrochemical signature of the groundwater. The TDS of the groundwater increases towards lower altitude as the hydrochemical facies changes along its flow paths. The

low TDS and bicarbonate groundwater type in the highland part indicate the fast hydrogeological regime of the plateau receiving a relatively high volume of precipitation. The TDS content increases along the flow direction as water flows from the recharge to the discharge areas. In the study area, Ca–Mg– HCO_3 is the dominant water type in the basic volcanics and Na– HCO_3 in the acidic volcanic rocks. In general, the TDS increases from the infiltration area along the watershed on the plateau to the drainage area formed by the valleys of the Robi River, Shenkorge River, and their tributaries (Fig. 4).

Fig. 6 A schematic cross section (W–E), showing the hydrogeological conceptual model of the Debre Sina landslide. The location of the cross section and its view direction is shown in Fig. 3



From west to east, the Na^+ concentration increases due to cation exchange. Similarly, there is a facies change, from being slightly mineralized in the west, to a significantly mineralized water type in the east. High Na^+ and K^+ concentrations in springs located in the lower part of the landslide show that the water was in contact with acidic volcanic rocks at the head scarp. In addition to cation exchange, weathering of silicate minerals controls the hydrogeochemical facies. The hydrochemical data provided useful insight into the main hydrogeochemical processes involved in the water mineralization. Water groups represented by Ca-Mg-HCO_3 are weakly mineralized waters within the basaltic and scoriaceous aquifers. Water groups represented by Ca-Na-HCO_3 and Ca-HCO_3 are draining the fractured rhyolites, ignimbrites, tuff, and trachytes, and, as could be expected, have a more dilute chemistry. The Na-Ca-Mg-HCO_3 and Ca-Na-Mg-HCO_3 water types are mixtures of the water types Ca-Na-HCO_3 and Ca-HCO_3 . Ca-Mg-HCO_3 and Ca-HCO_3 groups represent shallow groundwater circulation and short residence time that contain early stages of geochemical evolution (recent recharge) or rapidly circulating groundwater that has not undergone significant rock–water interactions (Edmunds and Smedley 2000; Kebede et al. 2005, 2008). The location of the landslide occurs within a formation that is poorly welded and composed of tuffaceous material that readily weathers to clay minerals and is capped by pervious basalt and/or ignimbrite and colluvial deposits (Fig. 6).

Mechanisms controlling water chemistry

Gibbs plots are employed to understand the processes affecting the geochemical parameters of groundwater (Gibbs 1970, 1971). In these diagrams, TDS is plotted against the concentrations of $\text{Na}^+ / (\text{Na}^+ + \text{Ca}^{2+})$ for cations, as well as TDS versus $\text{Cl}^- / (\text{Cl}^- + \text{HCO}_3^-)$ concentrations for anions. From these diagrams the natural mechanism controlling groundwater chemistry, including the rock-weathering dominance, evaporation and precipitation dominance, can be derived. The Gibbs plot of samples from the study area (Fig. 7) shows that all of the groundwater samples fall into the rock-weathering dominance group. The results indicate that the surface water had active interaction with groundwater, since the samples are not located in the rainfall dominance cell. All data points in the domain of water–rock interaction (Fig. 7a,b) indicate that chemical weathering controls water chemistry. As stated in the preceding, the interaction between rocks and water results in leaching of ions into the groundwater system, which influences the water chemistry. The chemistry of the spring water is mainly controlled by the residence time and the intensity of recharge. The upslope springs show low-mineralized water types, whereas the springs at the toe of the landslide area show higher mineralized water.

The implications of groundwater dynamics with respect to landslides

Hierarchical cluster analysis (HCA) is a typical multivariate statistical algorithm that puts observed data into meaningful clusters in their hierarchical order (Davis 2002). Three groundwater groups have been identified from the preliminary HCA based on major-ion chemistry (Na^+ , K^+ , Mg^{2+} , Ca^{2+} , HCO_3^- , SO_4^{2-} , F^- , Cl^-) of the water samples collected in this study (Fig. 8). The groundwater samples from the higher-altitude areas lie within the low-EC group I (Fig. 8). Most samples that lie in this group are characterized by low concentrations of all major ions. These samples are located in the highlands bounding the Rift Valley and are characterized by low salinity, with TDS below 216 mg/L. They were collected mainly from basaltic and scoriaceous aquifers, indicating fast groundwater flow. The vertical/subvertical joints and tensional fractures create a favourable condition for rainwater percolation. This area is generally acting as a recharge zone for the surface water as well as subsurface water that flows to the down-slope areas. This low EC (72–222 $\mu\text{S}/\text{cm}$) characteristic arises from the sample-point location within the recharge area (low residence time) and the presence of aquifer material with lower solubility, indicating that groundwater in the highland areas is getting recharge from rainwater. The samples in group II have an EC range of 115–465 $\mu\text{S}/\text{cm}$ and low concentrations of all the major ions similar to group I, but they are found at middle altitudes. These samples were collected close to the escarpments, and recharge seems to have taken place by precipitation over the highlands and transported through large faults. They were collected from highly fractured and shattered ignimbrite, rhyolite, trachyte associated with basalt, indicating that the groundwater movement is shallow to intermediate. However, they have relatively higher concentrations of Na^+ , K^+ , Cl^- and SO_4^{2-} as compared to group I, which is mainly related to the solution or interaction between water and secondary minerals or clay that precipitate into faults. The local freshwaters in the middle altitude are controlled by the normal faults ultimately derived from fast circulating recharge from the high rainfall of the plateau. Groundwater mainly emerges as high-discharge cold springs on the slope and at the bottom hill of the escarpment formed by steep faults. The groundwater samples in group II therefore correspond to groundwater in the intermediate flow systems. In the middle part of the study area, transitional types Ca-Na-HCO_3 and Ca-HCO_3 occur.

The water samples of group III were collected from the lower-elevation areas (below 1,500 m asl) in the eastern and northeastern parts of the study area, which are covered with volcanic ash-dominated units and sporadic colluvial-alluvial deposits. In these litho-units, the groundwater movement is slow, which together with the presence of soluble minerals, enhances the effects of rock–water interaction giving rise to relatively higher concentrations of Na^+ , K^+ , Cl^- and SO_4^{2-} .

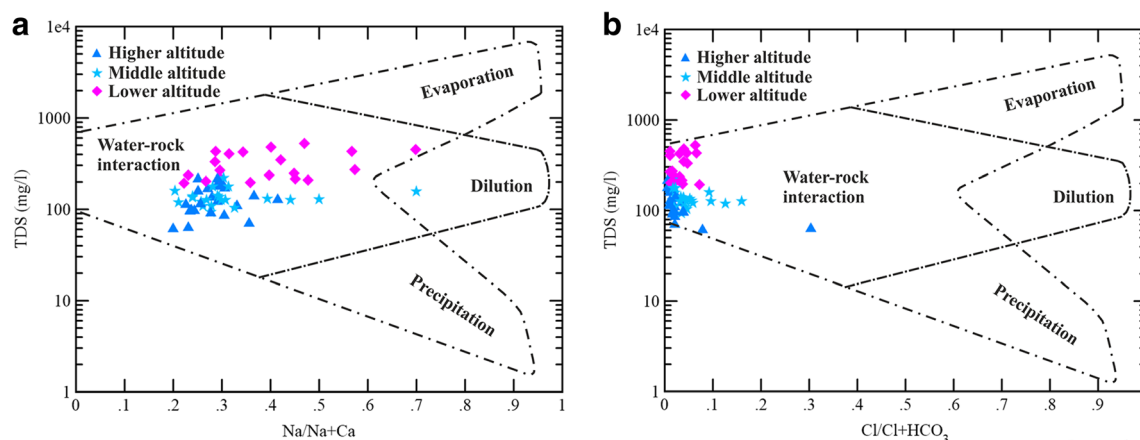


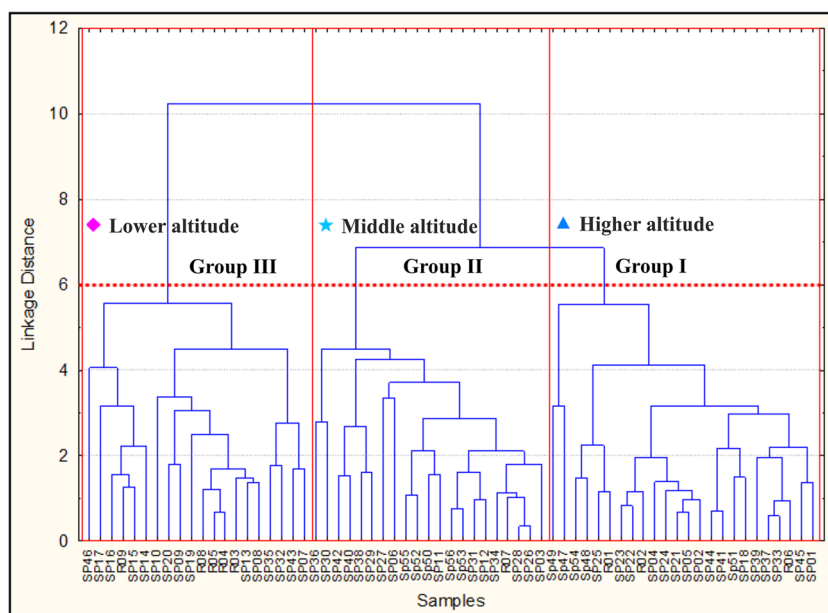
Fig. 7 Gibbs diagrams for **a** cations and **b** anions indicating rock–water interaction as the major process regulating the chemistry of the groundwater in the study area

The EC values of the groundwater samples within this group are between 215 and 573 $\mu\text{S}/\text{cm}$ and increase towards the Shewa Robit Valley, which indicates that there is intermediate to deep groundwater circulation and relatively higher residence time of the groundwater. The low hydraulic gradient of the groundwater in the lowland plain (Fig. 4) also indicates slow groundwater velocity. This leads to the longer residence time and enhancement of rock–water interaction. Sodium bicarbonate-rich groundwaters as well as higher sulphate concentrations were found in this discharge area; however, there are also localized freshwaters at the lower elevation, indicating that there is also fast circulating recharge from the high rainfall of the plateau along regional faults.

The average isotopic composition of the water samples collected from the study area is -5.70‰ for δD and -3.31‰ for $\delta^{18}\text{O}$, which is not very far from the long-term

weighted average isotope composition of the summer rainfall for Addis Ababa IAEA station (Kebede et al. 2008). This suggests that the groundwaters in the study area are mainly recharged from the summer rainfall on the highlands under cold air conditions. Therefore, they are generally of meteoric origin and they are not affected by some processes (like evaporation) during or before recharge. The residence time is short, the soil/rock–water interaction is low, and the water is little mineralized mainly in the highland and intermediate regions. Therefore, it is possible to conclude that the main cause of the landslide is not the active soil/rock–water interaction. It is rather because of the steep slope topography and the pressure formed during precipitation, which leads to an increase in the weight of the loose and weathered materials (increasing its shear stress). The material loses its shear resistance which finally results in land mass failure or landslide. The springs

Fig. 8 Categorization of the water samples resulting from a preliminary hierarchy cluster analysis (HCA) based on major ions chemistry using the complete linkage rule and Euclidean distances



and water ponding in the study area are usually seen at the upper failure section or main scarp of landslides, and their discharge comes from the overlying unit with a high discharge (Fig. 9).

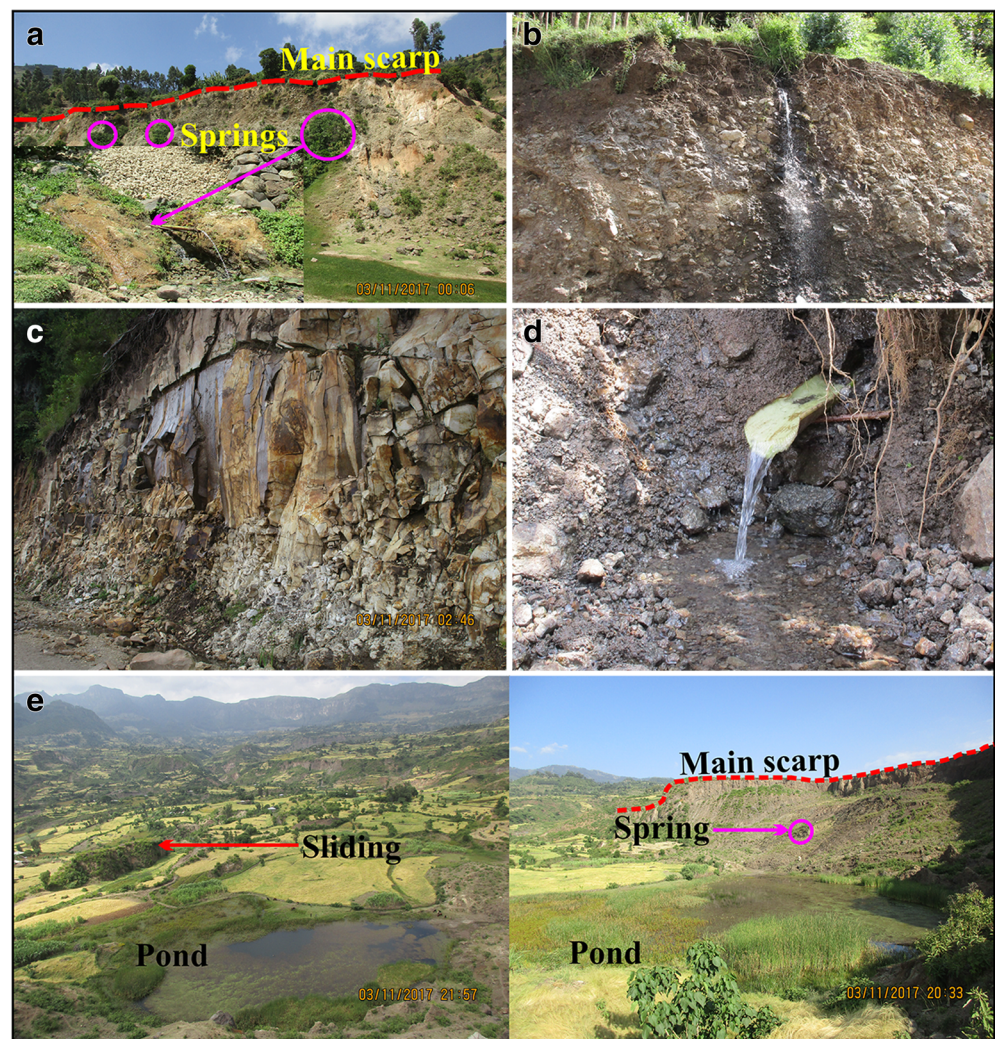
Intermittent springs emerge along the highly conductive layers of porphyritic-agglomeratic basalt, as well as where there is an intersection with the low-conductivity pyroclastic layers (groups I and II; Fig. 9). In areas where such highly permeable zones/layers are covered by colluvium, the groundwater can build up pore-water pressure from below and favour the triggering of shallow landslides. Below the spring horizons, humid zones are also formed which could additionally favour landslide triggering, especially during heavy or long-term rainfall. Such ponded water (Fig. 9e) can infiltrate into the slope and increase pore-water pressure, which decreases the shear strength, thereby causing instability to the slopes. In many of the landslide-affected sites, springs and seepage zones were observed to emerge along more fractured zones of the rocks or along the coarser soil horizons (Fig. 9a–d).

Evidence from isotopic signatures

Groundwater recharge

Groundwater recharge depends on the intensity of rainfall, permeability of the lithological units, and the topography that controls the groundwater infiltration and surface runoff. Knowing the origin of groundwater can help to understand the cause of the slope instabilities and to evaluate the influence of water on the moving mass. Groundwater recharge in the study area is mainly from precipitation. The water vapour from the moisture sources undergoes isotope fractionation before becoming rainfall during transportation towards the continent (Dansgaard 1964). During this process, δD and $\delta^{18}O$ values in rainwater can be correlated with the relationship $\delta D = 8\delta^{18}O + 10$, given by the GMWL (Craig 1961); furthermore, the isotopic composition of rainfall is dependent on a number of factors such as altitude, latitude, season, temperature and rainfall amount (Ayenew et al. 2008; Girmay et al.

Fig. 9 Pictures of typical landslide localities in the Debre Sina area: **a** emerging springs in ignimbrite-volcanic ash/tuff, **b** spring water at the contact of the top layer (colluvium) and underlying altered tuff, **c** seepage spring at the highly fractured ignimbrite, **d** spring water outflows from the bottom of the landslide and **e** ponded spring water at the toe of the landslide



2015). The $\delta^{18}\text{O}$ and δD values in the study area range from -0.73 to -5.08‰ and from 8.21 to -15.2‰ , with average values of -3.31 and -5.70‰ , respectively (Table 1). The d-excess value in the studied water samples ranges from 11.6 to 27.6‰ . Significant evaporation from surface waters might have caused the higher d-excess as the vapour recondenses in the atmosphere (Clark and Fritz 1997). The cross plot of $\delta^{18}\text{O}$ and $\delta^2\text{H}$ values of the water samples collected in the study (Fig. 10a) shows that local precipitation is the major source of recharge to the aquifers of the area. Slight shifting

of groundwater samples towards the left in ellipses A and B (Fig. 10a) is mainly attributed to their location at a higher altitude, and hence, the combined influence of the altitude and the difference in isotopic composition of its local air mass from that of Addis Ababa (Girmay et al. 2015). As a result of the cold and humid summer weather of the relatively elevated localities in the area, a depleted and high d-excess air mass is expected below the cloud base (Girmay et al. 2015). Addis Ababa is located close to the lakes region of the Ethiopian Rift Valley and, hence, the isotopic exchange of rain droplets with

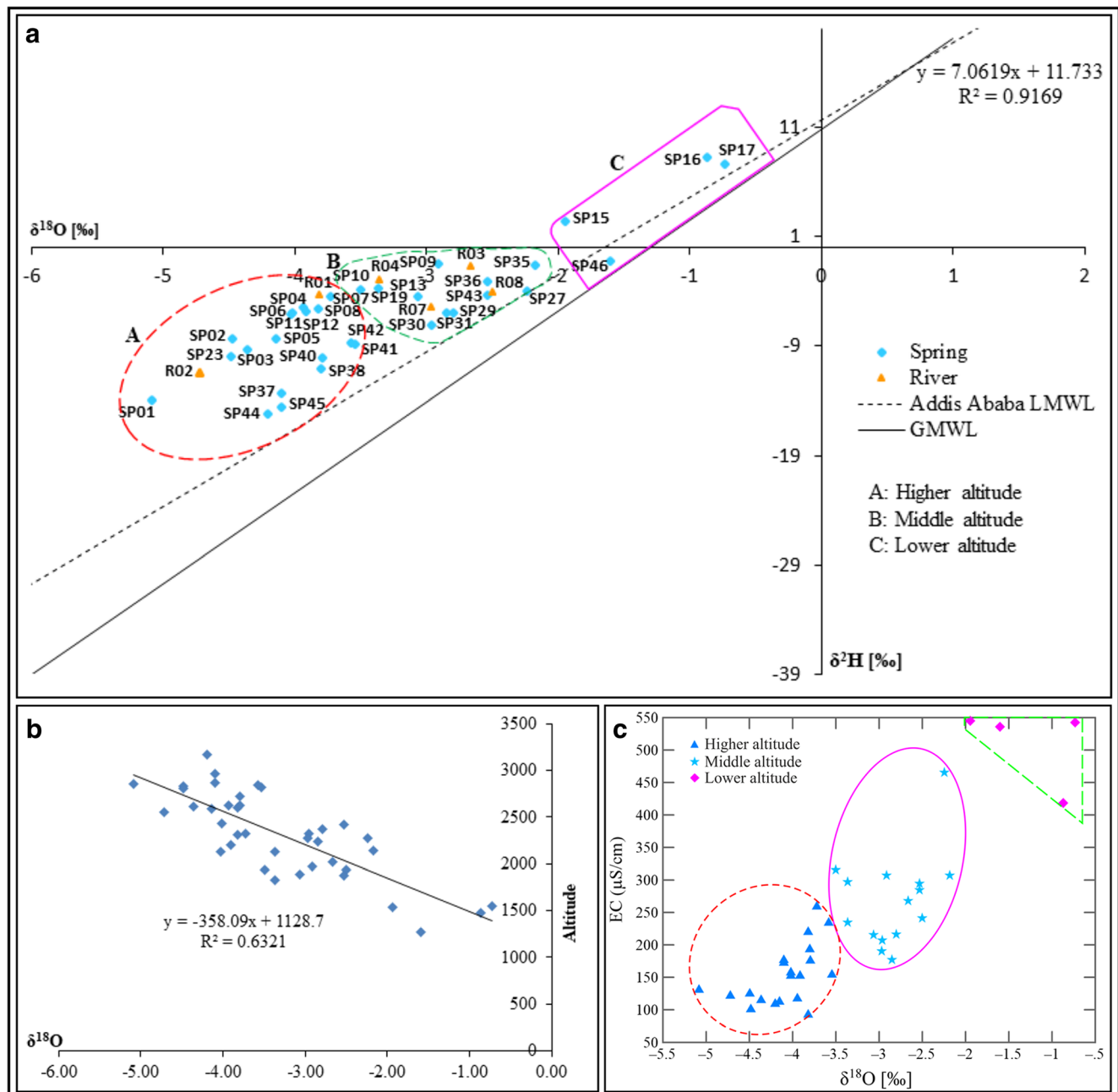


Fig. 10 **a** Cross plot of $\delta^{18}\text{O}$ versus $\delta^2\text{H}$ of the water samples with the Addis Ababa LMWL and the GMWL, **b** isotopic altitude effect of precipitation of the study area and **c** cross plot of $\delta^{18}\text{O}$ versus electrical conductivity (EC) of the study area

the relatively enriched vapour from these continental water bodies can result in a relatively enriched precipitation and groundwater recharge (Kebede et al. 2005).

The samples in ellipse A are at a relatively higher altitude than those in ellipse B, as demonstrated by more depleted samples in ellipse A, whereby the samples in A, B and C approximately correspond to the cluster groups I, II and III. The distance effect can also have a slight impact, as the area is located far from the moisture source of the summer precipitation in this region as compared to Addis Ababa. Kebede et al. (2005) also indicated that the major source of recharge to the Ethiopian groundwater is the summer rainfall, and the distance and altitude effects are prominent factors in depleting the precipitation in the central highlands of Ethiopia. The depleted signature of the samples SP07, SP09, SP10, SP13, R03, and R07 are similar to the others in ellipse B, while they are from relatively lower altitudes, which indicates that there is fast groundwater flow along regional open fractures. The enrichment of some spring samples in polygon C (Fig. 10a) signifies the influence of local recharge from nearby surface waters. In most cases, the springs and surface water on the landslide areas are being supplied with groundwater that is recharged from higher elevations above the landslide complex. During the fieldwork, interviews with local residents in the recently affected area indicate that numerous springs emerged at Yizaba, Shotel Amba, Nech Amba, Nib Amba, and Wanza Beret localities (Fig. 3) following the landslide incidents. And the springs in Yizaba locality are observed to change their flow directions from time to time which can indicate that there is still active mass movement in the area. Many landslides have occurred within the formation that is poorly welded and composed of tuffaceous and volcanic ash materials, which readily weather to clay minerals and are capped by highly brecciated ignimbrite. Springs are common at the interface between the fractured rock and its underlying weathered part or volcanic ash or a paleosol that occurs between various lava flows. The pyroclastic unit contains lapilli tuff, tuff breccia and tuffaceous strata, which are susceptible to slaking. Thus, the stable isotope results indicate that rainfall is one of the main triggering factors of the slope instability in the area associated with degrading rock mass strength and increase of the weight of the slope mass, i.e. increasing the pull of gravity.

The possibility of identifying a relationship between rainfall and reactivations of the landslide was investigated by using historic records of precipitation in the area. The mean annual precipitation measured in Debre Sina station for the period 1974–2016 was 1,812 mm, while the mean precipitation in the period from June to September was 1,037 mm. Figure 11 shows that the rainfall intensity in July and August of the years 2005, 2006, 2007 and 2014 was considerably above average. The most evident landslide reactivations were the movements that occurred in the summer

season of the years 2005–2007, 2014 and 2016 following long-lasting and above average precipitation (Fig. 11).

According to Woldearegay (2008) and Abay and Barbieri (2012), the ultimate mobilization of the landslides in the area has occurred in the month of September and some in October signifying the effect of the heavy rains on stability. Ayalew (1999) also found significant landslides in the Ethiopian highlands occurring between September and October. The water enters through the open tensional cracks or pipes during periods of high precipitation, building up a rapid pore-water pressure. This phenomenon, together with the effect of surface erosion around the lower parts of the slopes and an increase in bulk density at the top, might cause sudden and catastrophic failure.

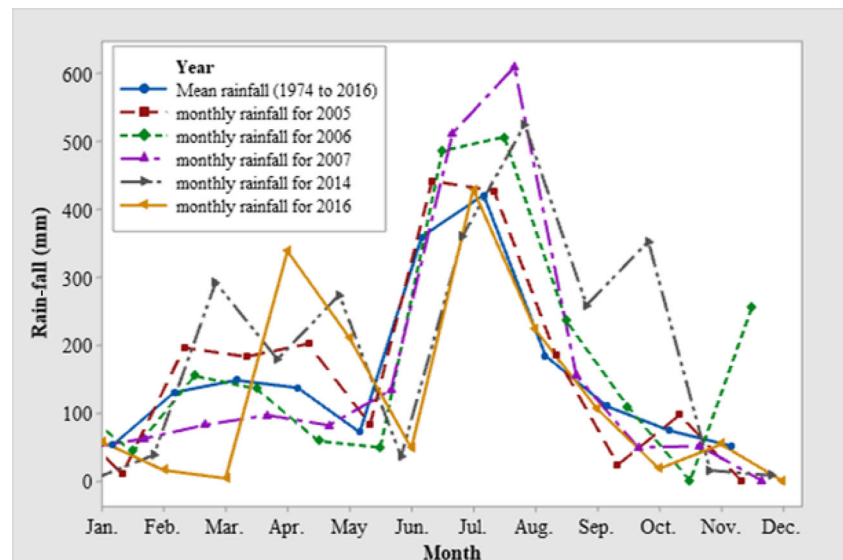
Spatial distribution of $\delta^{18}\text{O}$

The $\delta^{18}\text{O}$ of groundwater samples and the altitude from which they are collected, are inversely related and the regression line on the cross plot indicates a depletion rate of $-0.1\text{‰}/100\text{ m}$ for $\delta^{18}\text{O}$ (Fig. 10b). A similar altitude/pseudo-altitude effect in the Rift Valley was also reported by Kebede and Travi (2012). At lower altitudes clouds are usually higher above the ground level than at higher altitudes; therefore, the evaporative enrichment during rainfall is larger at low altitudes, which is called a pseudo-altitude effect (Kebede and Travi 2012; Girmay et al. 2015). Thus, the depletion in $\delta^{18}\text{O}$ of the shallow groundwater in the highland plateau of the study area (Fig. 10b) is due to recharge from already depleted precipitation reaching these elevated ground areas due to the altitude effect; however, the enrichment of shallow groundwater in the middle and lower altitudes (Fig. 10b) of the area can also be attributed to recharge from already enriched local rainfall. For river water, as it moves towards the eastern lower altitudes, progressive enrichment is also likely due to continuous evaporation as the surface-water flows downstream and further evaporation of the shallow groundwater that feeds the base flow in the discharge areas in the lower parts of Dem Aytamashy, Robi, Majete, and Shenkorge rivers and their tributaries (Fig. 4). This altitude-isotopic composition relationship can contribute to understanding the origin and flow paths of water within a slope. The EC versus oxygen isotope ($\delta^{18}\text{O}$) also shows a strong correlation (Fig. 10c) which can indicate the dominance of locally recharged shallow groundwater flow system in the area.

Vertical electrical sounding

Geophysical studies were carried out at two selected sites, namely, Yizaba and Armaniya. Vertical electrical soundings (VES) were conducted along the deep-seated landslide in Yizaba and along the shallow to intermediate landslide in Armaniya in order to trace the orientation and location of the faults and geological contacts, which can have considerable

Fig. 11 Mean monthly rainfall of the area for the last 43 years (1974–2016) and mean monthly rainfall for the years 2005, 2006, 2007, 2014 and 2016 for the Debre Sina area



effect on the groundwater circulation, as well as to map the various aquifer systems. These investigations were also aimed at determining the thickness of the overburden materials, to characterize the vertical distributions of subsurface layers, to estimate the depth to the water table, to identify probable

aquifer beds and to characterize the nature of the bedrock. The VES interpretation of the three profiles is based on lithological outcrops, surface observations and the overall geological setup of the area.

Fig. 12 **a** Geoelectrical section and **b** apparent pseudo-depth section along profile line-1

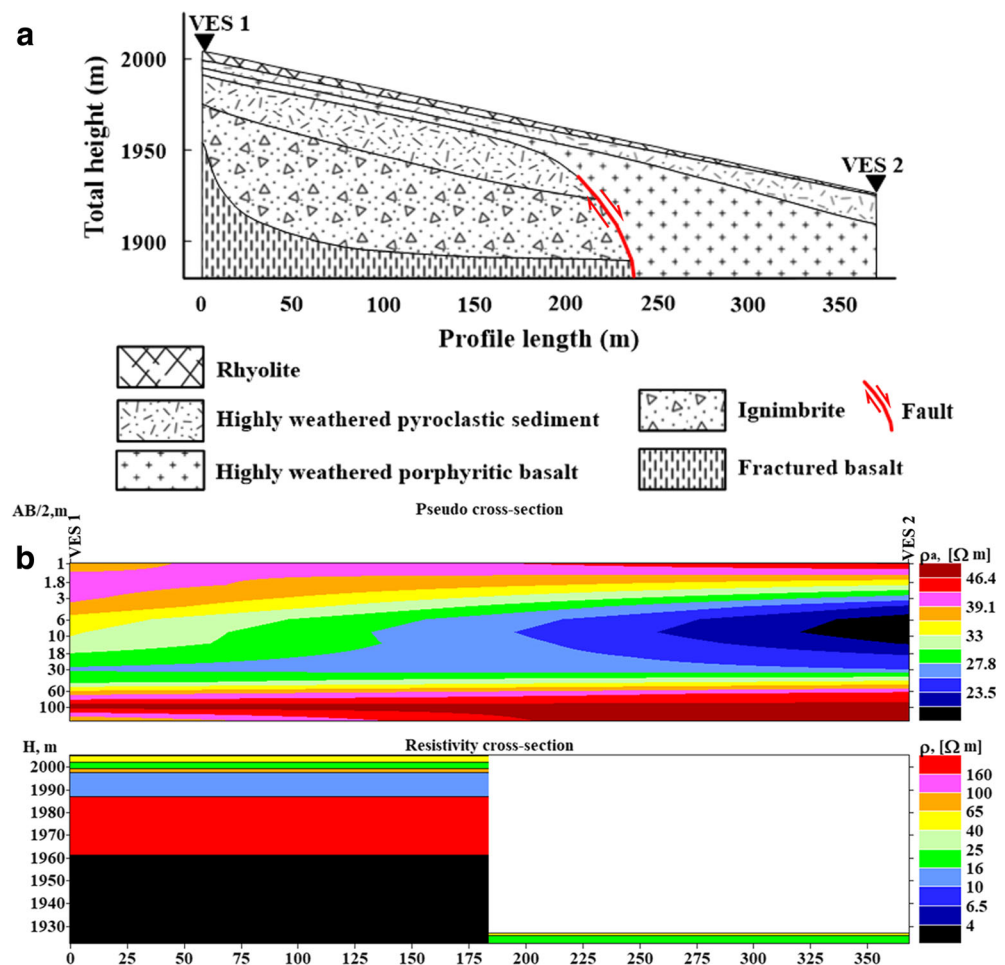
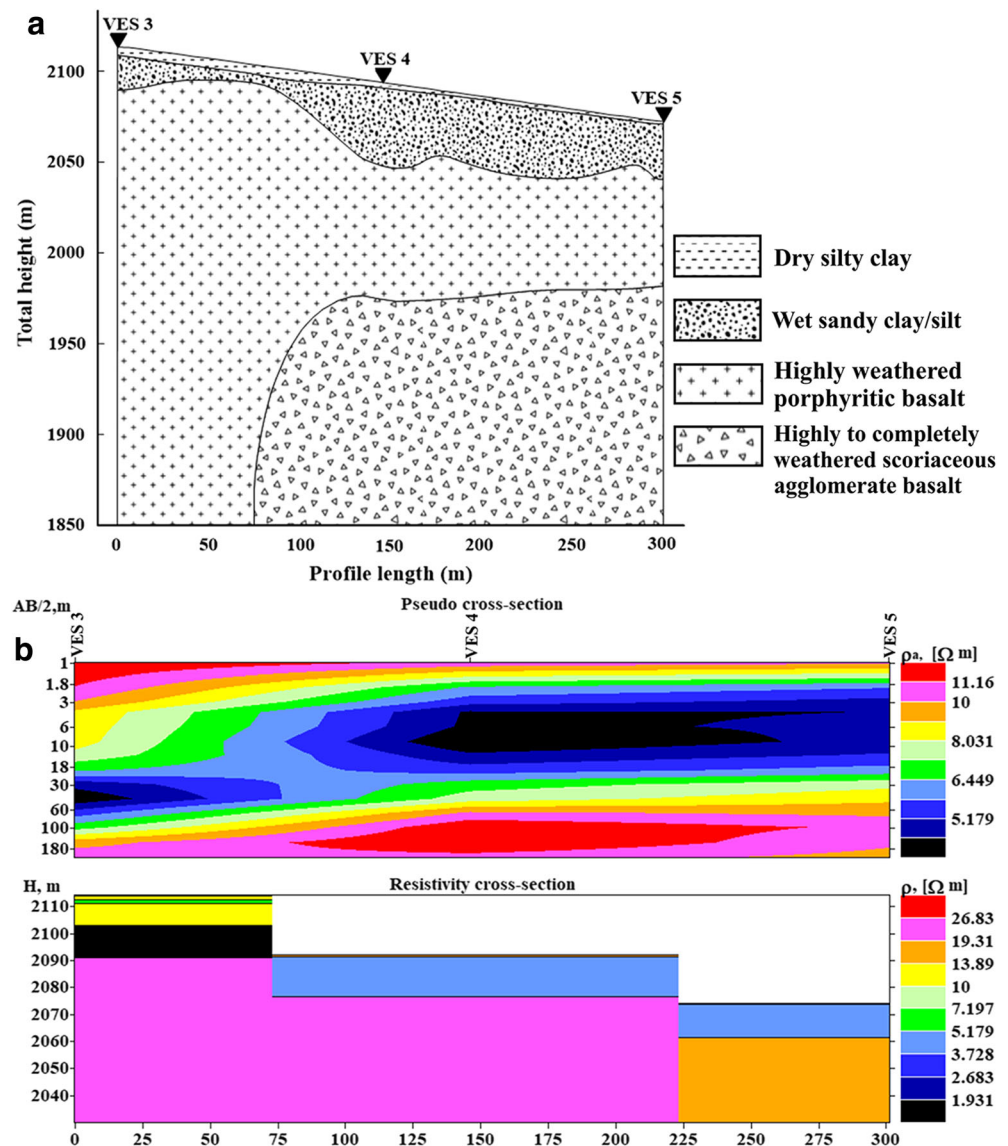


Fig. 13 **a** Geoelectrical section and **b** apparent pseudo-depth section along profile line-2



Profile line-1

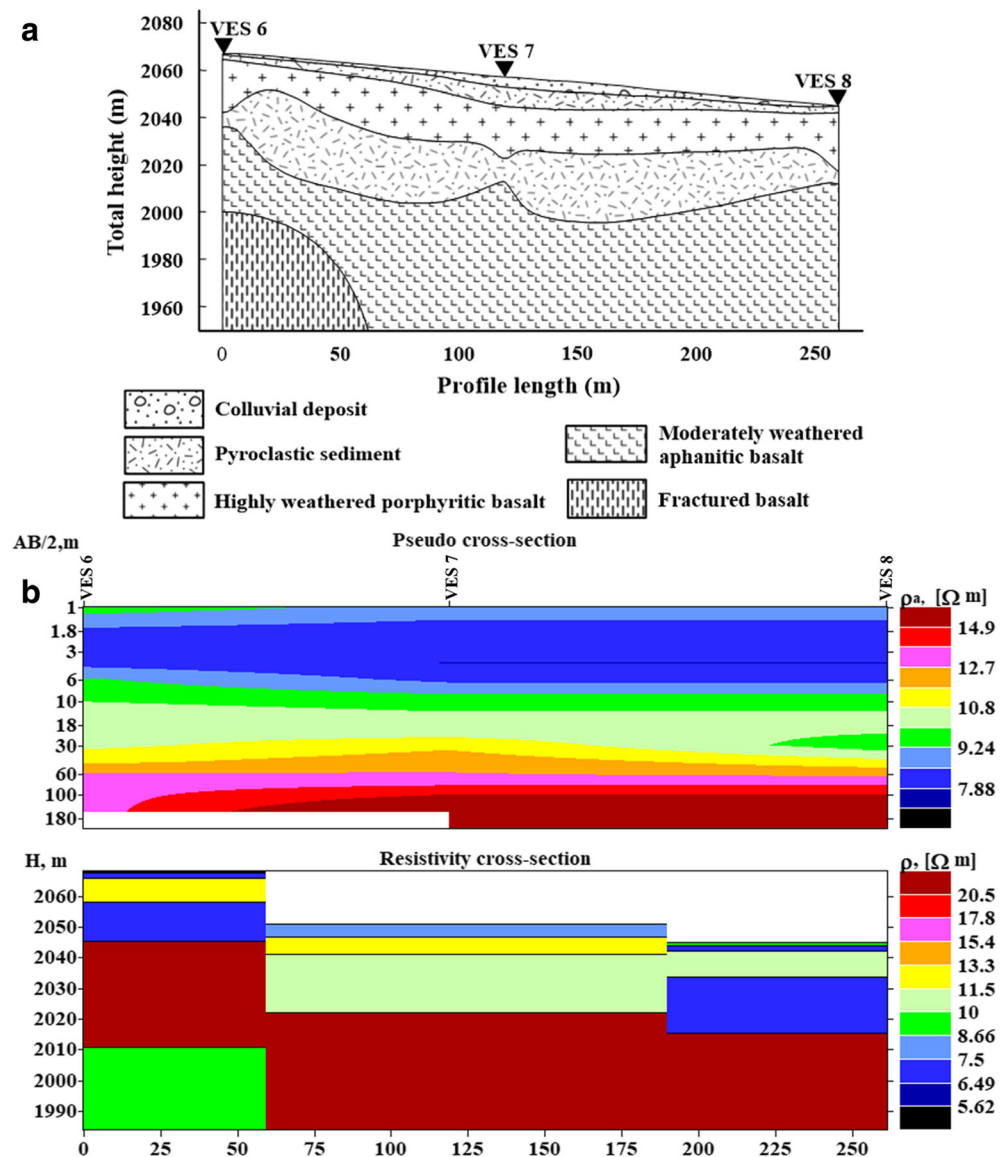
This profile line is about 368 m long and comprising two VES points: VES-1 and VES-2 (Fig. 3 shows profile line-1, and Fig. 12 shows the VES points). This profile shows a subsurface represented by six distinct major lithological units. The upper layer with a thickness range of 0.947–2.97 m and resistivity range of 40.2–47.4 $\Omega\text{-m}$ is interpreted as rhyolite. The second layer, having a resistivity response range of 19.1–23.7 $\Omega\text{-m}$ and a thickness range of 2.5–14.4 m, is interpreted as highly weathered pyroclastic sediment. The third layer, which has shown a resistivity range of 64.6–98 $\Omega\text{-m}$, is the highly weathered porphyritic basalt. The fourth layer, with a resistivity of 10.8 $\Omega\text{-m}$ and 10.5 m thickness, is attributed to the highly weathered pyroclastic sediment, which is inferred to be highly saturated. The fifth layer, with a resistivity of 207 $\Omega\text{-m}$ and has 25.9 m thickness, is attributed to ignimbrite.

In the locality around VES-1, the beds with relatively high resistivity rest on a formation characterized by a low-resistivity response (1.72 $\Omega\text{-m}$). This low resistivity can be explained by the highly fractured and saturated nature of the fractured basalt. Depth to the compact rock varies due to the presence of deep-seated geological structures. The layers from fourth to sixth have vanished in VES-2 because of the normal fault. The locality around VES-2 is observed to be vulnerable to sliding, which is possibly favoured by increased groundwater pressure within the fault zone. The measured resistivity values of the different geological units coincide with the previously obtained resistivity values in the literature (Keller and Frischknecht 1966).

Profile line-2

The pseudo-depth section and resistivity section for profile line-2, displayed in Fig. 13, allowed qualitative data to be

Fig. 14 **a** Geoelectrical section and **b** apparent pseudo-depth section along profile line-3



interpreted, based on both lateral and vertical resistivity variations in the subsurface. This line is about 300.5 m long, comprising three VES points: VES-3, VES-4, and VES-5 (Figs. 3 and 13). The profile covers the landslides in the Armaniya area (Fig. 3), displaying four layers that have distinct resistivity values reflecting variation in grain size, moisture content and weathering condition of the underlying rocks. The top thin layer, with a resistivity range of 14.5–25 Ω -m and thickness range of 0.4–2.92 m, represents dry silty clay soil. The second layer is characterized by very low resistivity values (4.3–5.99 Ω -m) and its thickness varies from 1.5 m to 14.8 m and is interpreted to be saturated sandy clay/silt soil. The third layer has shown a resistivity range of 10.37–19.67 Ω -m and 8.0–104 m thickness range and is associated with the highly weathered porphyritic basalt. The fourth layer, which has low resistivity (1.13–2.49 Ω -m), is the response of the highly fractured and saturated nature of the highly to

completely weathered scoriaceous agglomerate basalt. Great thicknesses of disturbed and sliding soils are located in the localities around VES-3 and VES-4, which could be due to the presence of thick saturated soils and the high degree of weathering and fracturing and the saturated nature of the underlying rocks.

Profile line-3

Profile line-3 is about 260.5 m long, comprising three VES points: VES-6, VES-7, and VES-8 (Figs. 3 and 14). This section reveals six layers with a resistivity variation between 6.7 and 28.9 Ω -m. Accordingly, the top thin layer, with resistivity values between 9.0 and 14.1 Ω -m and 0.43–4.23 m thickness range, is associated with the upper poorly sorted colluvial deposit, whereas the second layer, having a resistivity range of 6.7–12.2 Ω -m and 1.75–5.48 m thickness is

associated with the highly weathered pyroclastic sediment (tuff). The third layer, with a resistivity range of 10.1–12.6 Ω -m and 7.72–19.2 m thickness range, is attributed to the highly weathered porphyritic basalt, while the fourth layer, having a relatively low resistivity (7.12–7.26 Ω -m) and thickness range of 12.8–18.1 m, is interpreted as pyroclastic sediment; this low resistivity within the profile is possibly due to the intensive degree of weathering and saturated nature of the layer. The fifth layer, which has a resistivity response of 20.6–28.9 Ω -m, is interpreted as moderately weathered aphanitic basalt and has a thickness ranging between 28.6–34.4 m. The bottom-most layer has a resistivity of 9.05 Ω -m, which is lower than that of the overlying layer, is associated with the water-bearing fractured basalt. The fragile state of the bedrocks accelerates the rock mineral weathering by facilitating water ingress into the rock mass.

Generally, all the aforementioned interpreted geophysical data indicate that the area is covered by unconsolidated sediments and highly decomposed and weak volcanic rocks that are susceptible to sliding when they get moist. The heterogeneity of the geological materials and the presence of relatively impermeable layers embodied within the highly permeable volcanic rocks can result to the build-up of high water pressure at the interface between the contrasting permeability layers, which can trigger landslides. On the other hand, the intense fracturing in the tilted basalt and ignimbrite beds can create weak zones that accelerate the infiltration of water which can be responsible for the build-up of high hydrostatic pressure, resulting in lowering of the effective normal stresses in the rock mass, giving rise to landslides.

Conclusions

The hydrogeology in the volcanic areas in the western part of the study area is very complex as the lithology is disrupted by cross-cutting faults and interrupted by volcanic structures. As can be seen from the chemical characterization, shallow to intermediate aquifers cause groundwater flow into the landslide mass, influencing long-term groundwater-level fluctuations underneath the landslide and, as a consequence, its stability. The low TDS and bicarbonate types (Ca–Mg–HCO₃ and Ca–HCO₃) of groundwater chemistry indicate a fast hydrogeological regime receiving a relatively high amount of precipitation with infiltrated water flowing in the fissured and disturbed aquifers developed in various volcanic rocks and intercalated sediments. The slight rock–water interaction has shaped the groundwater chemistry, as shown by the ionic ratios and Gibbs plots. A Piper plot depicts that groundwater types of the study area are Ca–Mg–HCO₃, Ca–HCO₃, Ca–Mg–Cl–SO₄ and Na–HCO₃. Groundwater shows a systematic change in hydrochemical facies along the groundwater flow direction from the highland area towards the lowland area. The

dominantly depleted isotopic signatures in the study area indicate that the high amount of precipitation in the cool and humid highlands is the main source of both the groundwater and surface water in the area. In the highland areas, the groundwater storage and flow are predominantly in fault zones and joints, resulting in little contact between the groundwater and the geological materials. Two groundwater flow systems (shallow/local and intermediate-deep) are identified in the study area. The chemical and isotopic characterization indicates that shallow to intermediate aquifers cause groundwater flow into the landslide mass, influencing long-term groundwater-level fluctuations underneath the landslide and, as a consequence, its stability.

The VES investigation in the Armaniya and Yizaba areas indicates that the landslide is a deep-seated feature incorporating both bedrock and surficial deposits. There are many springs and seepage zones along the contact between the basalt and ignimbrite beds with the pyroclastic sediments (volcanic ash). The heterogeneity of the geological materials and the presence of relatively impermeable layers embodied within the highly permeable volcanic rocks can result in the build-up of high water pressure at the interface between the contrasting permeability layers, which can trigger landslides. On the other hand, the intense fracturing in the tilted basalt and ignimbrite beds can create weak zones that accelerate the infiltration of water, which can be responsible for the build-up of high hydrostatic pressure resulting in lowering of the effective normal stresses in the rock mass giving rise to landslides. Furthermore, the concave shape of a terrain can enhance the convergence of groundwater flow into the landslide area since groundwater levels are relatively high in such terrains. In general, the main triggering factors for landslide problems in the area are the intensive weathering of the rocks; the prominent geological structures; steep slope and gradient; heavy rainfall; the groundwater pressure developed during precipitation; and the presence of low-permeability beds which force the percolating water to flow laterally. This study has provided a good level of understanding of the effect of the hydrogeologic environment on landslide triggering.

Acknowledgments We highly appreciate Isodetec (Environmental Monitoring) in Munich and the Department of Materials and Earth Sciences at the Technical University of Darmstadt for analysing the water samples (stable isotopes $\delta^{18}\text{O}$ and δD). We also thank the three anonymous reviewers and the editors of *Hydrogeology Journal* for their constructive comments and suggestions.

Funding Open Access funding enabled and organized by Projekt DEAL. The first author would like to thank the German Academic Exchange Service (DAAD) for the scholarship grant to pursue the PhD study. This work was supported by the Ruhr University Research School PLUS, funded by Germany's Excellence Initiative (DFG GSC 98/3).

Open Access This article is licensed under a Creative Commons Attribution 4.0 International License, which permits use, sharing, adaptation, distribution and reproduction in any medium or format, as long as you give appropriate credit to the original author(s) and the source,

provide a link to the Creative Commons licence, and indicate if changes were made. The images or other third party material in this article are included in the article's Creative Commons licence, unless indicated otherwise in a credit line to the material. If material is not included in the article's Creative Commons licence and your intended use is not permitted by statutory regulation or exceeds the permitted use, you will need to obtain permission directly from the copyright holder. To view a copy of this licence, visit <http://creativecommons.org/licenses/by/4.0/>.

References

- Abay A, Barbieri G (2012) Landslide susceptibility and causative factors evaluation of the landslide area of Debrešina, in the southwestern Afar escarpment, Ethiopia. *J Earth Sci Eng* 2:133–144
- Abebe B, Dramis F, Fubelli G, Umer M, Asrat A (2010) Landslides in the Ethiopian highlands and the rift margins. *J African Earth Sci* 56: 131–138. <https://doi.org/10.1016/j.jafrearsci.2009.06.006>
- Ayalew L (1999) The effect of seasonal rainfall on landslides in the highlands of Ethiopia. *Bull Eng Geol Environ* 58:9–19. <https://doi.org/10.1007/s100640050065>
- Ayalew L (2000) Factors affecting slope stability in the Blue Nile basin. *Landslides in Research, Theory and Practice, Proceedings of the 8th International Symposium on Landslides*, 26–30 June 2000 (Cardiff: Thomas Telford), pp 101–106
- Ayalew L, Yamagishi H (2002) Landsliding and landscape development: the case of northern Ethiopia. In: *Proceedings of the international congress intrapraevent 2002*, Matsumoto, Japan, pp 595–606
- Ayenew T (2005) Major ions composition of the groundwater and surface water systems and their geological and geochemical controls in the Ethiopian volcanic terrain. *SINET Ethiop J Sci* 28:171–188. <https://doi.org/10.4314/sinet.v28i2.18253>
- Ayenew T, Barbieri G (2005) Inventory of landslides and susceptibility mapping in the Dessie area, northern Ethiopia. *Eng Geol* 77:1–15. <https://doi.org/10.1016/j.enggeo.2004.07.002>
- Ayenew T, Kebede S, Alemayehu T (2008) Environmental isotopes and hydrochemical study applied to surface water and groundwater interaction in the Awash River basin. *Hydrol Process* 22:1548–1563. <https://doi.org/10.1002/hyp.6716>
- Bogaard TA, Antoine P, Desvarreux P, Giraud A, Van Asch WJ (2000) The slope movements within the Mondorès graben (Drôme, France): the interaction between geology, hydrology and typology. *Eng Geol* 55:297–312
- Calmels D, Galy A, Hovius N, Bickle M, West AJ, Chen MC, Chapman H (2011) Contribution of deep groundwater to the weathering budget in a rapidly eroding mountain belt, Taiwan. *Earth Planet Sci Lett* 303:48–58
- Cervi F, Ronchetti F, Martinelli G, Bogaard A, Corsini A (2012) Origin and assessment of deep groundwater inflow in the Ca' Lita landslide using hydrochemistry and in situ monitoring. *Hydrol Earth Syst Sci* 16:4205–4221. <https://doi.org/10.5194/hess-16-4205-2012>
- Chernet T, Travi Y, Valles V (2001) Mechanism of degradation of the quality of natural water in the lakes region of the Ethiopian Rift Valley. *Water Res* 35:2819–2832. [https://doi.org/10.1016/S0043-1354\(01\)00002-1](https://doi.org/10.1016/S0043-1354(01)00002-1)
- Clark I, Fritz P (1997) *Environmental isotopes in hydrogeology*. Lewis, Boca Raton, FL
- Craig H (1961) Isotopic variations in meteoric waters. *Science* 133(3465):1702–1703. <https://doi.org/10.1126/science.133.3465.1702>
- Dansgaard BW (1964) Stable isotopes in precipitation. *Tellus* 16(4):436–468. <https://doi.org/10.3402/tellusa.v16i4.8993>
- Darling WG, Gizaw B, Arusei MK (1996) Lake-groundwater relationships and fluid-rock interaction in the East African Rift Valley: isotopic evidence. *J African Earth Sci* 22:423–431. [https://doi.org/10.1016/0899-5362\(96\)00026-7](https://doi.org/10.1016/0899-5362(96)00026-7)
- Davis JC (2002) *Statistics and data analysis in geology*. Wiley, New York
- de Montety V, Marc V, Emblanch C, Malet JP, Bertrand C, Maquaire O, Bogaard TA (2007) Identifying the origin of groundwater and flow processes in complex landslides affecting black marls: insights from a hydrochemical survey. *Earth Surf Process Landf* 32:32–48
- Di Maio C, Santoli L, Schiavone P (2004) Volume change behaviour of clays: the influence of mineral composition, pore fluid composition and stress state. *Mech Mater* 36:435–451
- Di Maio C, Scaringi G, Vassallo R (2014) Residual strength and creep behaviour on the slip surface of specimens of a landslide in marine origin clay shales: influence of pore fluid composition. *Landslides* 12:657–667. <https://doi.org/10.1007/s10346-014-0511-z>
- Edmunds WM, Smedley PL (2000) Residence time indicators in groundwater: the East Midlands Triassic sandstone aquifer. *Appl Geochem* 15:737–752. [https://doi.org/10.1016/S0883-2927\(99\)00079-7](https://doi.org/10.1016/S0883-2927(99)00079-7)
- Edmunds WM, Darling WG, Kinniburgh DG, Kotoub S, Mahgoub S (1992) Sources of recharge at Abu Delaig. *Sudan J Hydrol* 131:1–24. [https://doi.org/10.1016/0022-1694\(92\)90211-D](https://doi.org/10.1016/0022-1694(92)90211-D)
- Epstein S, Mayeda T (1953) Variation of O-18 content of waters from natural sources. *Geochim Cosmochim Acta* 4:213–224
- Gaucher ÉC, Blanc P, Bardot F, Braibant G, Buschaert S, Crouzet C, Altmann S (2006) Modelling the porewater chemistry of the Callovian–Oxfordian formation at a regional scale. *C R Geosci* 338:917–930
- Gibbs RJ (1970) Mechanisms controlling world water chemistry. *Science* 170:1088–1090. <https://doi.org/10.1126/science.170.3962.1088>
- Gibbs RJ (1971) Mechanisms controlling world water chemistry: evaporation–crystallization process. *Science* 172:871–872
- Girmay E, Ayenew T, Kebede S, Alene M, Wöhlisch S, Wisotzky F (2015) Conceptual groundwater flow model of the Mekelle Paleozoic–Mesozoic sedimentary outlier and surroundings (northern Ethiopia) using environmental isotopes and dissolved ions. *Hydrogeol J* 23:649–672. <https://doi.org/10.1007/s10040-015-1243-4>
- Guglielmi Y, Bertrand C, Compagnon F, Follacci JP, Mudry J (2000) Acquisition of water chemistry in a mobile fissured basement massif: its role in the hydrogeological knowledge of the La Clapière landslide (Mercantour Massif, southern Alps, France). *J Hydrol* 229:138–148
- Guglielmi Y, Vengeon JM, Bertrand C, Mudry J, Follacci JP, Giraud A (2002) Hydrogeochemistry: an investigation tool to evaluate infiltration into large moving rock masses (case study of La Clapière and Se'chillienne alpine landslides). *Bull Eng Geol Environ* 61:311–324
- IAEA (2020) Global Network of Isotopes in Precipitation (GNIP). International Atomic Energy Agency. <http://www.iaea.org/water>. Accessed December 2020
- IPI2Win-1D Program (2003) Programs set for 1-D VES data interpretation. Dept. of Geophysics, Geological Faculty, Moscow University, Moscow, Russia
- Iverson RM (2000) Landslide triggering by rain infiltration. *Water Resour Res* 36:1897–1910. <https://doi.org/10.1029/2000WR900090>
- Kebede S, Travi Y (2012) Origin of the d18O and d2H composition of meteoric waters in Ethiopia. *Quaternary International* 257:4–12. <https://doi.org/10.1016/j.quaint.2011.09.032>
- Kebede S, Travi Y, Alemayehu T, Ayenew T (2005) Groundwater recharge, circulation and geochemical evolution in the source region of the Blue Nile River. *Ethiopia. Appl Geochem* 20(9):1658–1676. <https://doi.org/10.1016/j.apgeochem.2005.04.016>
- Kebede S, Travi Y, Asrat A, Alemayehu T, Ayenew T (2008) Groundwater origin and flow along selected transects in Ethiopian

- rift volcanic aquifers. *Hydrogeol J* 16:55–73. <https://doi.org/10.1007/s10040-007-0210-0>
- Keller GV, Frischknecht FC (1966) *Electrical methods in geophysical prospecting*. Pergamon, Oxford, 519 pp
- Lindenmaier F, Zehe E, Dittfurth A, Ihringer J (2005) Process identification at a slow-moving landslide in the Vorarlberg Alps. *Hydrol Process* 19:1635–1651
- Malet JP (2003) Les “glissements de type écoulement” dans les marnes noires des Alpes de Sud. Morphologie, fonctionnement et modélisation hydro-mécanique [Thèse]: Université Louis Pasteur - Strasbourg 1, pp 364
- Mebrahtu TK, Hussien B, Banning A, Wöhlisch S (2020) Predisposing and triggering factors of large-scale landslides in Debre Sina area, central Ethiopian highlands. *Bull Eng Geol Environ* 80:1–19. <https://doi.org/10.1007/s10064-020-01961-1>
- Mebrahtu TK, Alber M, Wöhlisch S (2020b) Tectonic conditioning revealed by seismic refraction facilitates deep-seated landslides in the western escarpment of the Main Ethiopian Rift. *Geomorphology* 370:107382. <https://doi.org/10.1016/j.geomorph.2020.107382>
- Nyssen J, Moeyersons J, Poesen J, Deckers J, Haile M (2003) The environmental significance of the remobilisation of ancient mass movements in the Atbara-Tekeze headwaters, northern Ethiopia. *Geomorphology* 49:303–322. [https://doi.org/10.1016/S0169-555X\(02\)00192-7](https://doi.org/10.1016/S0169-555X(02)00192-7)
- Picarelli L, Urciuoli G, Mandolini A, Ramondini M (2006) Softening and instability of natural slopes in highly fissured plastic clay shales. *Nat Hazards Earth System Sci* 6:529–539
- Piper AM (1944) A graphic procedure in the geochemical interpretation of water analyses. *EOS Trans Am Geophys Union* 25:914–923. <https://doi.org/10.1029/TR025i006p00914>
- Temesgen B, Mohammed MU, Korme T (2001) Natural hazard assessment using GIS and remote sensing methods, with particular reference to the landslides in the Wondogenet area, Ethiopia. *Phys Chem Earth, Part C Solar, Terr Planet Sci* 26:665–675. [https://doi.org/10.1016/S1464-1917\(01\)00065-4](https://doi.org/10.1016/S1464-1917(01)00065-4)
- Tóth J (1999) Groundwater as a geologic agent: an overview of the causes, processes, and manifestations. *Hydrogeol J* 7:1–14
- Tullen P, Parriaux A, Tacher L (2002) Improvement of the hydrogeological modelling of landslides. In: *Engineering geology for developing countries*. Balkema, Rotterdam, pp 1406–1414
- Vallet A, Bertrand C, Mudry J, Bogaard T, Fabbri O, Baudement C, Régent B (2015) Contribution of time-related environmental tracing combined with tracer tests for characterization of a groundwater conceptual model: a case study at the Séchillienne landslide, western Alps (France). *Hydrogeol J* 23:1761–1779. <https://doi.org/10.1007/s10040-015-1298-2>
- Wang CH, Kuol CH, Peng TR, Chen WF, Liu TK, Chiang CJ, Liu WC, Hung JJ (2001) Isotope characteristics of Taiwan groundwaters. *Western Pacific Earth Sci* 1(4):415–428
- Woldearegay K (2008) Characteristics of a large-scale landslide triggered by heavy rainfall in Tarmaber area, central highlands of Ethiopia. *Geophys Res Abstr* 10:EGU2008-A-04506-EGU02008
- Woldearegay K (2013) Review of the occurrences and influencing factors of landslides in the highlands of Ethiopia: with implications for infrastructural development. *Momona Ethiopian J Sci* 5:3–31
- Woldearegay K, Schubert W, Klima K, Mogessie A (2005) Landslide hazards mitigation strategies in the northern highlands of Ethiopia. In: *Proceedings of the International Conference on Landslide Risk Management, Vancouver, BC, 31 May–3 June 2005*
- Zvelebil J, Šima J, Vilímek V (2010) Geo-risk management for developing countries: vulnerability to mass wasting in the Jemma River basin, Ethiopia. *Landslides* 7(1):99–103. <https://doi.org/10.1007/s10346-009-0191-2>

Publisher's note Springer Nature remains neutral with regard to jurisdictional claims in published maps and institutional affiliations.